

Gaussian Universality in Neural Network Dynamics with Generalized Structured Input Distributions

Jaeyong Bae

Department of Physics, Korea Advanced Institute of Science and Technology, Daejeon 34141, Republic of Korea

Hawoong Jeong*

*Department of Physics, Korea Advanced Institute of Science and Technology, Daejeon 34141, Republic of Korea and
Center of Complex Systems, Korea Advanced Institute of Science and Technology, Daejeon 34141, Republic of Korea*

Bridging the gap between the practical performance of deep learning and its theoretical foundations often involves analyzing neural networks through stochastic gradient descent (SGD). Expanding on previous research that focused on modeling structured inputs under a simple Gaussian setting, we analyze the behavior of a deep learning system trained on inputs modeled as Gaussian mixtures to better simulate more general structured inputs. Through empirical analysis and theoretical investigation, we demonstrate that under certain standardization schemes, the deep learning model converges toward Gaussian setting behavior, even when the input data follow more complex or real-world distributions. This finding exhibits a form of universality in which diverse structured distributions yield results consistent with Gaussian assumptions, which can support the theoretical understanding of deep learning models.

I. INTRODUCTION

The study of artificial neural networks through the lens of statistical physics has a well-established history. Neural networks trained on samples from a distribution have traditionally been analyzed as optimization problems within complex systems [2–12]. These problems are generally classified based on the learning process, whether the entire dataset or a subset is used per iteration, as in gradient descent and batch gradient descent, respectively, or whether a single sample is used per iteration, as in stochastic gradient descent (SGD, also known as on-line learning).

When the entire dataset is used, one can fix the dataset size and interpret the neural network and corresponding loss function as analogous to a spin system and potential energy. The replica method can then be employed to investigate the system. This approach has provided successful interpretations of simple one- or two-layer perceptrons during the early development of neural networks [3–6], and more recently has demonstrated applicability to more advanced settings including generative models [13–15].

On the other hand, when considering SGD, where a single dataset is used per iteration, the neural network variables are updated to optimize the loss for each sample. The behavior of neural networks under such independent random sampling can be described without the need for the replica method. By analyzing the equations of motion derived from this approach, it is possible to track generalization error and the time evolution of specific weights in the neural network [7–12].

Recently, the composition of the input dataset has become a crucial consideration. Studies have shifted

focus toward understanding neural network behavior under structured input data [1, 16–21]. The notion of structured data posits that despite the high-dimensional nature of typical datasets (such as MNIST in Deng [22] with 28×28 dimensions and CIFAR in Krizhevsky [23] with $3 \times 32 \times 32$ dimensions), they can often be distilled into lower-dimensional representations. For instance, in the MNIST dataset, the digits display structured patterns like lines and curves rather than random pixel arrangements. This characteristic of low-dimensional structural features in data has been discussed in numerous studies [24–29].

Motivated by the presence of these low-dimensional structures, recent research has explored the impact of processing such structured inputs on deep learning. Specifically, theoretical analyses have modeled inputs with a simple Gaussian distribution [1, 19, 20]; however, such theoretical approaches are still limited in their ability to capture the complexities of real-world data, which are often better represented by Gaussian mixtures rather than simple Gaussian distributions [30–32].

Our study aims to extend the simple Gaussian framework by examining neural network dynamics when inputs are characterized by Gaussian mixtures in low dimensions. We analyze how neural network behavior changes as the underlying distribution shifts from simple Gaussian to a Gaussian mixture.

Our key findings are as follows:

- Standardization of input datasets modeled by Gaussian mixtures (or general distributions) in low dimensions results in convergence with the dynamics observed under Gaussian inputs.
- The observed convergence is largely due to the weakly correlation condition of dataset and model settings. With the standardization, weakly correlated random variables combinations converge to

* hjeong@kaist.edu

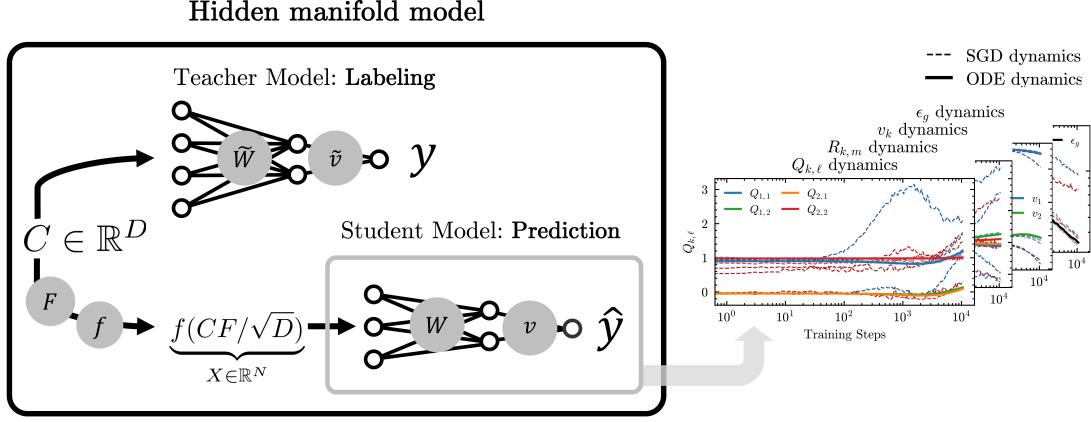


FIG. 1. Illustration of the hidden manifold model (Goldt *et al.* [1]) and our experimental scheme using Gaussian and Gaussian mixture inputs. The term *ODE dynamics* refers to the outcomes from ordinary differential equation (ODE) simulations, which align with SGD under a simple Gaussian input. In contrast, *SGD dynamics* describes the results obtained from running SGD with C from arbitrary distribution.

Gaussian, even under general distribution, by generalized central limit theorem.

This study is organized as follows. In Section II we provide a brief background on relevant studies, and in Section III we describe the Gaussian mixture settings and experimental conditions. In Section IV, we present the experimental results showcasing the patterns of convergence. Then in Section V we offer mathematical proof of the observed phenomena. In Section VI we discuss limitation and possible expansion of our results. Finally, we conclude our study in Section VII.

II. BACKGROUND

This Section II offers an overview of previous finding from Goldt *et al.* [1]. From the teacher-student model framework and one of its evolved variants, the hidden manifold model. We introduce their findings in neural network dynamics.

A. Hidden Manifold Model

The teacher-student model is a well-regarded method in the study of high-dimensional problems [33–36]. This model framework consists of a teacher model that generates dataset labels and a student model that learns the labels. In a two-layer neural network, the weights of the first and second layers of the teacher model are represented by matrices $\tilde{W} \in \mathbb{R}^{M \times D}$ and $\tilde{v} \in \mathbb{R}^{1 \times M}$, respectively. We define the activation function of the teacher model as \tilde{g} . Similarly, the weights of the first and second layers of the student model are denoted by $W \in \mathbb{R}^{K \times N}$ and $v \in \mathbb{R}^{1 \times K}$, with the activation function represented as g . In the canonical teacher-student model, the input $X \in$

\mathbb{R}^N is typically element-wise i.i.d. from a Gaussian distribution. But here, we aim for input characteristics that reflect intrinsic structural properties rather than being merely extrinsically Gaussian.

To embed these intrinsic properties into the input X , Goldt *et al.* [1] utilized a D -dimensional vector, $C \in \mathbb{R}^D$, that follows an element-wise i.i.d. Gaussian distribution. This is achieved through the feature matrix $F \in \mathbb{R}^{D \times N}$ and nonlinear function f as follows:

$$X = f(CF/\sqrt{D}) = f(U) \in \mathbb{R}^N. \quad (1)$$

By modeling the dataset in this manner, the input X intrinsically reflects the characteristics of C , which is distributed as Gaussian. Furthermore, the labels generated by the teacher model are derived not directly from X but from C , which reflects the dominance of the intrinsic characteristics in the true label.

In summary, the teacher-student model results can be expressed as follows:

$$y = \tilde{g}(\tilde{C}\tilde{W}^\top/\sqrt{D})\tilde{v}^\top, \quad \hat{y} = g(XW^\top/\sqrt{N})v^\top. \quad (2)$$

This model, recognizing a hidden structure in lower dimensions, is termed the hidden manifold model [1]; Fig. 1 shows a schematic of the model along with our experimental scheme (see Section IV). For the convenience of subsequent discussions, we denote the preactivations of the teacher and student models as ν and λ , respectively:

$$\begin{aligned} \nu &= C\tilde{W}^\top/\sqrt{D} \in \mathbb{R}^M, \\ \lambda &= XW^\top/\sqrt{N} = f(U)W^\top/\sqrt{N} \in \mathbb{R}^K. \end{aligned} \quad (3)$$

When input C spans beyond a singular data point to represent a dataset of size P , it assumes a matrix form, denoted as $C \in \mathbb{R}^{P \times D}$. Consequently, each preactivation is expressed through matrices $\nu \in \mathbb{R}^{P \times M}$ and $\lambda \in \mathbb{R}^{P \times K}$. In practice, the matrix form is commonly used. However,

for theoretical derivations, where the focus is on the underlying distribution properties rather than specific sampled instances, the vector form is preferred.

Without any additional notice, the notation $M_{i,j}$ represents the element located in the i -th row and j -th column of any given matrix M , and v_i denotes the i -th component of any vector v .

Below, we frequently consider an infinitely large dataset dimension N and intrinsic dimension D ($N \rightarrow \infty, D \rightarrow \infty$), a scenario often referred to as the thermodynamic limit from the perspective of statistical physics. To maintain consistency with prior studies, this research also adopts the term thermodynamic limit to describe the $N \rightarrow \infty, D \rightarrow \infty$ scenario.

B. Dynamics of Neural Network Weights

In this study, we adopt the approach of Goldt *et al.* [1] to update the student model weights using a scaled SGD under the quadratic loss $\mathcal{L} = 1/2(\hat{y} - y)^2$, with learning rate η . The updates are performed while considering the vector form of λ , ν and U ,

$$\begin{aligned} W_{k,i} &:= W_{k,i} - \frac{\eta}{\sqrt{N}} v_k (\hat{y} - y) g'(\lambda_k) f(U_i), \\ v_k &:= v_k - \frac{\eta}{N} g(\lambda_k) (\hat{y} - y). \end{aligned} \quad (4)$$

By defining the normalized number of steps as $t = 1/N$ in the thermodynamic limit $N \rightarrow \infty$, which can be interpreted as a continuous time-like variable, the updates transform into ordinary differential equations (ODEs).

For example, v_k satisfies the following ODE:

$$\frac{dv_k}{dt} = \eta \left[\sum_n^M \tilde{v}_n I_2(k, m) - \sum_j^K v_j I_2(k, j) \right], \quad (5)$$

where $I_2(k, m) = \mathbb{E}[g(\lambda_k) \tilde{g}(\nu_m)]$ and $I_2(k, j) = \mathbb{E}[g(\lambda_k) g(\lambda_j)]$ represent the correlations of functions.

Using a similar approach for v , we can derive the dynamics of our teacher-student model in the form of ODEs, as detailed in Appendix A. The dynamics are predominantly influenced by the correlations of specific functions, such as $I_2(k, m)$, and $I_2(k, j)$. To calculate these correlations of functions, referred to here as the *function correlation*, we require information on the underlying distribution of $\{\lambda, \nu\}$.

C. The Gaussian Equivalence Property

Goldt *et al.* [1] investigated the distribution of preactivations in hidden manifold model, $\{\lambda, \nu\}$ under certain assumptions. To summarize the previous findings, $\{\lambda, \nu\}$ follow a Gaussian distribution characterized by a specific covariance matrix.

As mentioned, to emphasize the distributional properties, we consider λ, ν in vector form. Assuming that the

weights W, \tilde{W} and feature matrix F do not significantly alter the input properties, having elements in $\mathcal{O}(1)$ scale, adopt the following assumptions

Assumption II.1. The feature matrix has bounded property,

$$\frac{1}{\sqrt{D}} \sum_{r=1}^D F_{r,i} F_{r,j} = \mathcal{O}(1), \quad \sum_{r=1}^D F_{r,i}^2 = D, \quad (6)$$

and

Assumption II.2. For all $p, q \geq 1$ and any indices $k_1, \dots, k_p, r_1, \dots, r_q$:

$$\frac{1}{\sqrt{N}} \sum_i W_{k_1,i} \dots W_{k_p,i} \times F_{r_1,i} \dots F_{r_q,i} = \mathcal{O}(1), \quad (7)$$

with the q and p distinct. A similar scaling holds for terms involving the teacher weights.

Under these conditions taken from Goldt *et al.* [1], we can approximately calculate the covariances of $\{\lambda, \nu\}$, i.e., $\mathbb{E}[\lambda_k \lambda_\ell], \mathbb{E}[\lambda_k \nu_m], \mathbb{E}[\nu_m \nu_n]$. This analysis enables the derivation of the asymptotic form of all covariance matrices of preactivations $\{\lambda, \nu\}$, where higher-order correlations vanish in the thermodynamic limit. The hidden manifold model setup (Section II A), e.g., the teacher model, the student model, or the feature matrix, satisfies these assumptions as shown by Goldt *et al.* [1].

Consequently, the preactivations follow a Gaussian distribution, a result summarized as the Gaussian equivalence property (GEP).

Property II.3 (Gaussian equivalence property (GEP)). *In the thermodynamic limit ($N \rightarrow \infty, D \rightarrow \infty$), with finite $K, M, D/N$, and under Assumption II.1 and Assumption II.2, if C follows a standard Gaussian distribution $\mathcal{N}(0, I)$, then $\{\lambda, \nu\}$ are jointly Gaussian variables of dimension $K + M$. This means that the statistics involving $\{\lambda, \nu\}$ are entirely represented by their mean and covariance.*

Property II.3 taken from Goldt *et al.* [1] states that the preactivation distribution $\{\lambda, \nu\}$ follows a joint Gaussian distribution. This property allows us to understand the student model's dynamics (e.g., student weight, generalization error) via the mean and covariance of the joint Gaussian distribution of preactivations. For example, the student weight dynamics (Eq. (5)) are tractable by calculating I_2 under the $\{\lambda, \nu\}$ distribution. Detailed derivations are provided in Appendix A.

Before expressing the covariance matrix, for convenience we redefine $\bar{\lambda}_k$ as

$$\bar{\lambda}_k = \frac{1}{\sqrt{N}} \sum_{i=1}^N W_{k,i} (f(U_i) - \mathbb{E}_{u \sim \mathcal{N}(0,1)}[f(u)]). \quad (8)$$

$\bar{\lambda}_k$ also follows a jointly Gaussian distribution with $\mathbb{E}[\bar{\lambda}_k] = 0$. Consequently, the new distribution $\{\bar{\lambda}, \nu\}$

has means of

$$\mathbb{E}[\bar{\lambda}_k] = \mathbb{E}[\nu_m] = 0, \quad (9)$$

and covariances as follows:

$$Q_{k,\ell} \equiv \mathbb{E}[\bar{\lambda}_k \bar{\lambda}_\ell] = (c - a^2 - b^2) \Omega_{k,\ell} + b^2 \Sigma_{k,\ell}, \quad (10)$$

$$R_{k,m} \equiv \mathbb{E}[\bar{\lambda}_k \nu_m] = b \frac{1}{D} \sum_{r=1}^D S_{k,r} \widetilde{W}_{m,r}, \quad (11)$$

$$T_{m,n} \equiv \mathbb{E}[\nu_m \nu_n] = \frac{1}{D} \sum_{r=1}^D \widetilde{W}_{m,r} \widetilde{W}_{n,r}. \quad (12)$$

Here, a , b , and c represent the statistical properties of the nonlinear function f , used in the transformation of student model inputs X , $X = f(CF/\sqrt{D})$, given as

$$a = \mathbb{E}[f(u)], \quad b = \mathbb{E}[uf(u)], \quad c = \mathbb{E}[f(u)^2], \quad (13)$$

under $u \sim \mathcal{N}(0, 1)$. The newly defined matrices satisfy the following relations:

$$S_{k,r} \equiv \frac{1}{\sqrt{N}} \sum_{i=1}^N W_{k,i} F_{r,i}, \quad (14)$$

$$\Omega_{k,\ell} \equiv \frac{1}{N} \sum_{i=1}^N W_{k,i} W_{\ell,i}, \quad (15)$$

$$\Sigma_{k,\ell} \equiv \frac{1}{D} \sum_{r=1}^D S_{k,r} S_{\ell,r}. \quad (16)$$

For compact notation, we focus on the symmetric nonlinear function f that satisfies $a = \mathbb{E}[f(u)] = 0$. These defined covariances capture the essential characteristics of the teacher-student model dynamics.

The student model learns by attempting to emulate the teacher model outputs. Each covariance matrix holds a distinct meaning in relation to the dynamics of the model. The matrix Q relates to the correlation among the student model's own preactivations, implying the dynamics of the first layer of the student model. The matrix R relates to the correlation between the preactivations of the student and teacher models, reflecting the student model's accuracy in mirroring the teacher. The matrix T remains constant throughout the learning process, serving as a mirror of the teacher model's inherent characteristics.

To summarize, within the context of the hidden manifold model characterized by a simple Gaussian distribution, the learning dynamics of the student model are primarily influenced by the function correlation terms. Such terms, which depend on the distributional properties of $\{\lambda, \nu\}$, can be calculated once the distribution is determined. Under Assumption II.1 and Assumption II.2, the GEP shows that the preactivations $\{\lambda, \nu\}$ follow a Gaussian distribution, allowing us to analytically dissect the dynamics of the student model.

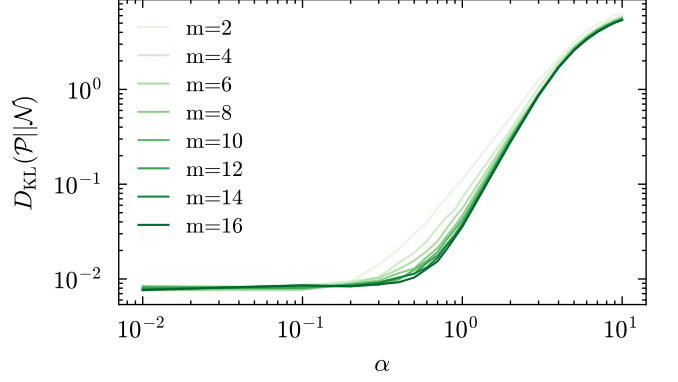


FIG. 2. Kullback-Leibler (KL) divergence $D_{\text{KL}}(\mathcal{P}||\mathcal{N})$ for different values of α and number of components m , where \mathcal{P} represents the Gaussian mixture distribution.

III. METHOD

In this section, we detail our approach to configuring Gaussian mixture inputs and our experimental settings, where we consider a two-layer teacher-student model as in Section A.

A. Gaussian Mixture Setting

In this study, we employ a generalized Gaussian mixture distribution as the teacher model input. To distinguish between Gaussian inputs and generalized Gaussian mixture inputs, we denote them as C and \mathcal{C} , respectively. Below, we describe the specific Gaussian mixture setting utilized in our analysis. Given that $C \in \mathbb{R}^{P \times D}$, we construct $\mathcal{C} \in \mathbb{R}^{P \times D}$, by first generating D different Gaussian mixture distributions, each with a fixed number of mixture components m . We then sample P values from each of these distributions. In other words, \mathcal{C}_r , $r = 1, 2, \dots, D$ is drawn from D different Gaussian mixture distributions. Each of the D Gaussian mixture distributions is generated under means μ_k by uniformly distributing them within the interval $[-\alpha, \alpha]$, and standard deviations σ_k by uniformly distributing them within the interval $(0, \beta)$. The weights π_k are randomly selected from a uniform distribution and normalized so that $\sum_k^m \pi_k = 1$. As summarize, each D Gaussian mixture distribution probability function is as follows:

$$p(\mathcal{C}_r) = \sum_{k=1}^m \pi_k \mathcal{N}(\mu_k, \sigma_k), \quad r = 1, 2, \dots, D. \quad (17)$$

With this D Gaussian mixture, we generate $\mathcal{C} \in \mathbb{R}^{P \times D}$ by sampling from each respective Gaussian mixture.

This methodology allows us to conduct empirical investigations across a spectrum of Gaussian mixtures by adjusting the parameters α , β and m . In Fig. 2, we check that increasing α under fixed $\sigma_k = 1$ leads to a monotonically increasing Kullback-Leibler (KL) divergence from a

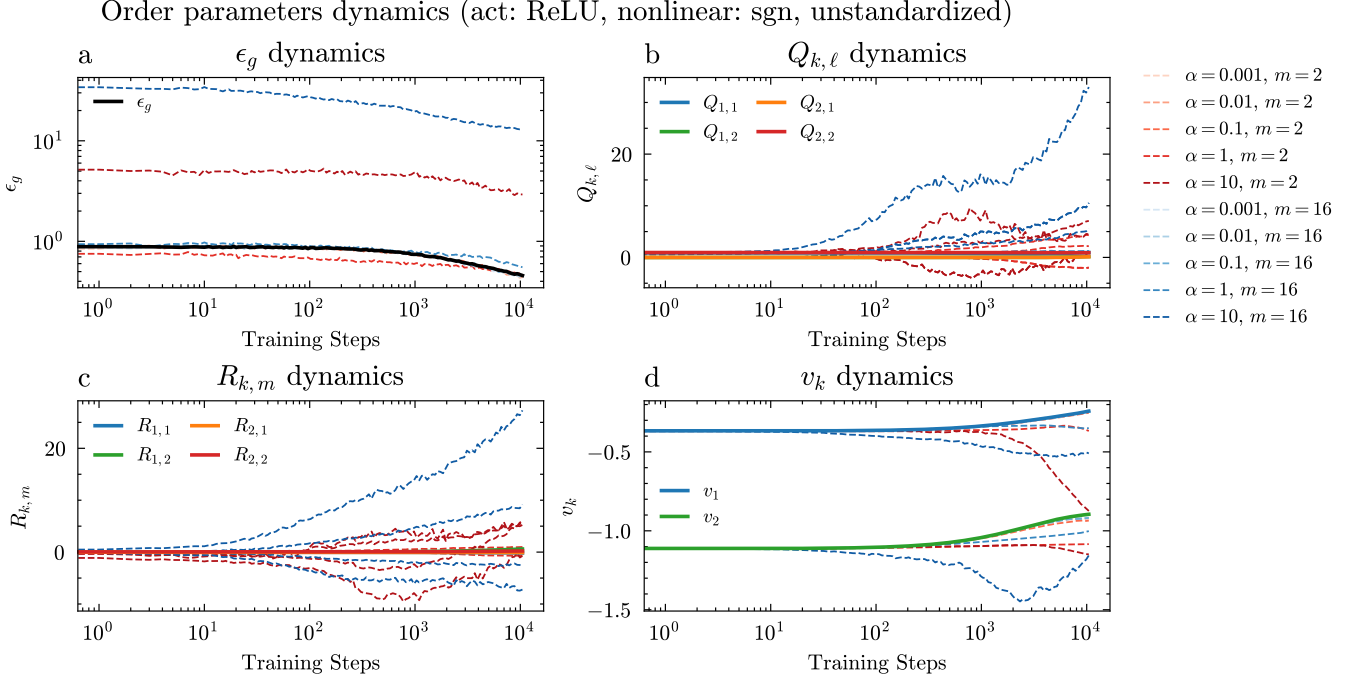


FIG. 3. Examples of dynamics under unstandardized Gaussian mixtures with $m = 2, m = 16$, and $\alpha = 0.001, 0.01, 0.1, 1, 10$. Dynamics of (a) generalization error ϵ_g , (b) covariance matrix Q , (c) covariance matrix R , and (d) weight of the second layer v . The SGD results are averaged over 10 runs.

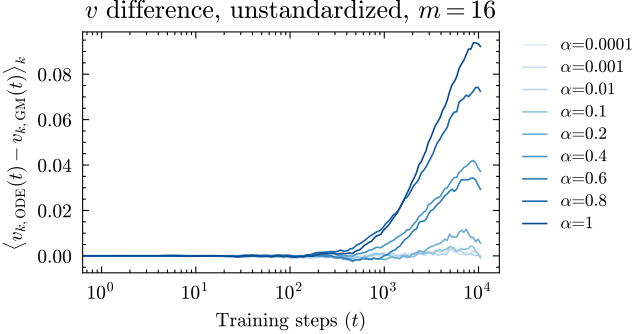


FIG. 4. Difference in v for various α values. $v_{k, \text{ODE}}$ refers to v_k values from ODE dynamics, and $v_{k, \text{GM}}$ refers to v_k values from SGD dynamics under the Gaussian mixture setting. The error due to simple randomness was corrected. Here, $\langle \cdot \rangle_k$ denotes the average over $k = 1, 2$, and t denotes the training steps for simplicity.

single Gaussian distribution. We estimate KL divergence by using k -nearest-neighbor distances [37].

B. Additional Experimental Settings

The dimension of teacher model input \mathcal{C} was set to $D = 500$, and the dimension of student model input X was set to $N = 1000$. The dimensions of the hidden layers for both teacher and student models were

uniformly set to $K = M = 2$. Both the teacher and student models employed the same activation function, $g(x) = \tilde{g}(x) = \text{ReLU}(x)$. The nonlinear function $f(x)$ used to generate the student input was $f(\cdot) = \text{sgn}(\cdot)$.

The learning rate was set to $\eta = 0.2$, and training was conducted using the quadratic loss $\mathcal{L} = \frac{1}{2}(\hat{y} - y)^2$ with a scaled SGD update procedure as shown in Eq. (4). The student model was updated for a total of 100×1000 steps. In various teacher model input \mathcal{C} , we used the same initial conditions ($\tilde{W}, \tilde{v}, W, v$ and F) to obtain the evolution of the dynamics. As results, we use fixed teacher model, student model and feature matrix in numerical simulation, determined as element drawn from i.i.d standard Gaussian, as hidden manifold model.

IV. RESULTS

In this section, we explore how the dynamics evolve as the input distribution transitions from simple Gaussian \mathcal{C} to a Gaussian mixture \mathcal{C} . In Section II we established that when input follows a simple Gaussian distribution, we can analytically trace the dynamics using the order parameters Q , R , and T alongside ODEs. The results derived from these ODEs are analytically consistent with those obtained through SGD under a simple Gaussian \mathcal{C} . Here, we compare the dynamics derived from ODE computations with those from SGD across various scenarios when inputs are \mathcal{C} . For simplicity, we use “ODE dynamics” to refer to the ODE simulation results, which are

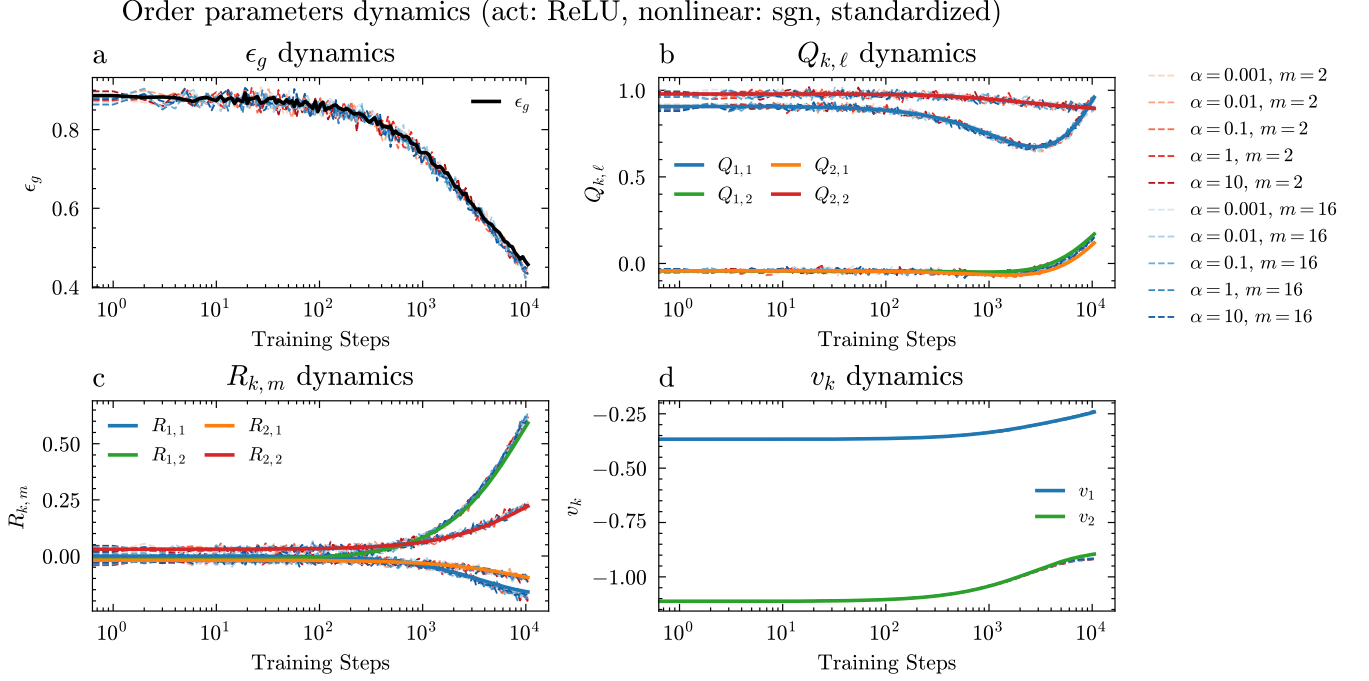


FIG. 5. Examples of dynamics under standardized Gaussian mixtures with $m = 2, m = 16$, and $\alpha = 0.001, 0.01, 0.1, 1, 10$. Dynamics of (a) generalization error ϵ_g , (b) covariance matrix Q , (c) covariance matrix R , and (d) weight of the second layer v . The SGD results are averaged over 10 runs.

essentially equivalent to SGD under C , and use “SGD dynamics” to denote the results obtained from running SGD with given C . Our primary focus is on the results obtained using the ReLU activation function and the sgn nonlinear function. For outcomes related to the erf activation function, refer to Appendix B.

Additionally, we examine two distinct scenarios regarding the teacher model’s input C : unstandardized and standardized. In the unstandardized scenario, C is directly sampled from the distribution. Conversely, in the standardized scenario, C is rescaled to have $\langle C \rangle \rightarrow 0$ and $\langle C^2 \rangle^{1/2} \rightarrow 1$ for each dimension. Here, $\langle X^n \rangle$ denotes the n -th cumulant of the random variable X . See Fig. 1 for our scheme to compare the ODE and SGD dynamics, which depends on the selection of samples at each update step, we run SGD multiple times from the same initial conditions—keeping the teacher model, student model, and feature matrix F fixed—while varying the random seed for sample selection. The resulting dynamics are then averaged to obtain a more stable representation.

A. Unstandardized Gaussian Mixture Results

First, we examine how the dynamics deviate when the inputs have various Gaussian mixture properties. We consider $\alpha = 0.001, 0.01, 0.1, 1, 10$ and $m = 2, 16$ with

fixed $\sigma_k = 1$ for visualization. As observed in Fig. 3, the dynamics under unstandardized Gaussian mixture settings significantly diverge from those under a simple Gaussian distribution. Although both the ODE dynamics and SGD dynamics start from identical initial conditions, significant discrepancies emerge over time. As α increases, the divergence becomes more pronounced, matching the KL divergence trends shown in Fig. 2, where α exhibits greater influence on KL divergence than does the component number m .

Even for an arbitrary distribution, the dynamics of the second layer’s weight v (Eq. (5)) maintain the same form but differ in the calculation of the function correlation. By tracking the difference in v between ODE and SGD dynamics, we can assess the effect of distribution differences.

In Fig. 4, we can see how the mean difference of v deviates over time; as expected, the deviation becomes more distinct as time evolves. The deviation is small when α is sufficiently small because the means μ_i for the Gaussian mixture are mostly sampled at 0, making it difficult to distinguish between samples from the Gaussian mixture and simple Gaussian distribution. This convergence due to distribution similarity occurs in the $\alpha \leq 0.1$ regime, where the KL divergence is on the order of $\mathcal{O}(10^{-2})$ (Fig. 2). Conversely, larger divergence in the dynamics is observed for large α , as increasing α enhances the dissimilarity between the Gaussian mixture and simple Gaussian distribution.

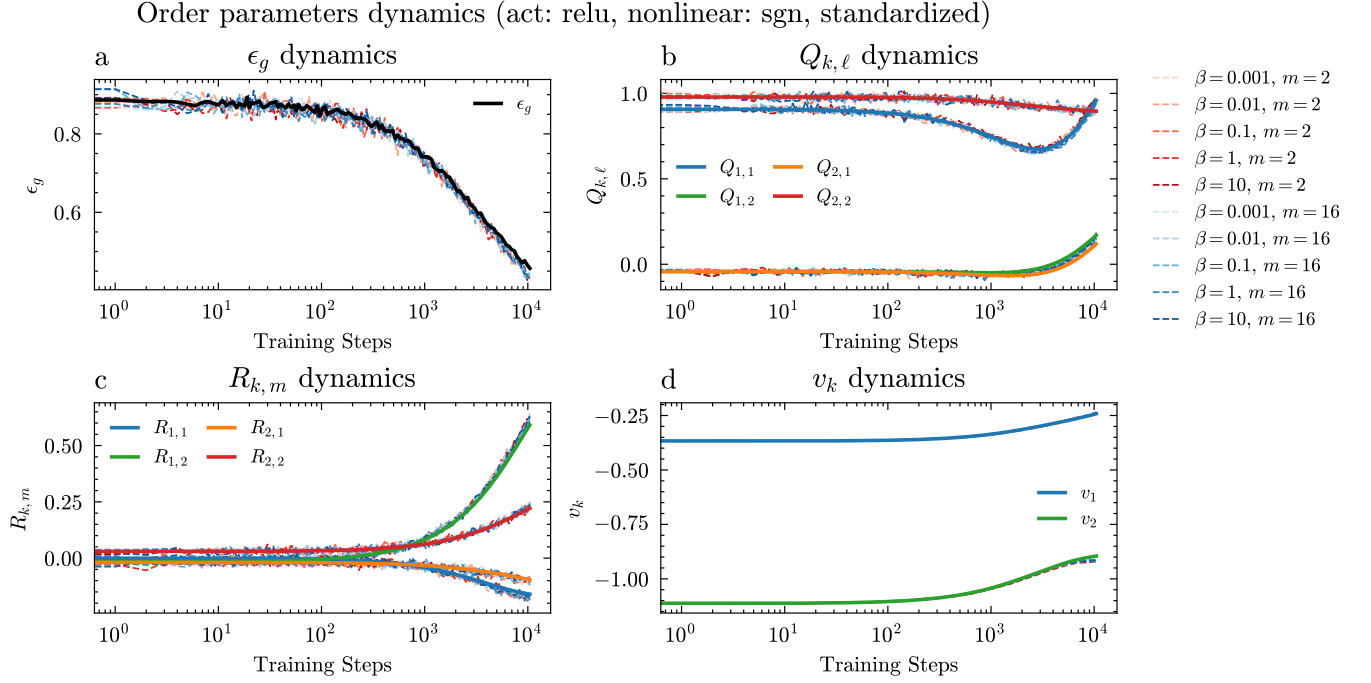


FIG. 6. Examples of dynamics under standardized Gaussian mixtures with $m = 2, m = 16$, $\alpha = 10$, and $\beta = 0.001, 0.01, 0.1, 1, 10$. Dynamics of (a) generalization error ϵ_g , (b) covariance matrix Q , (c) covariance matrix R , and (d) weight of the second layer v . The SGD results are averaged over 10 runs.

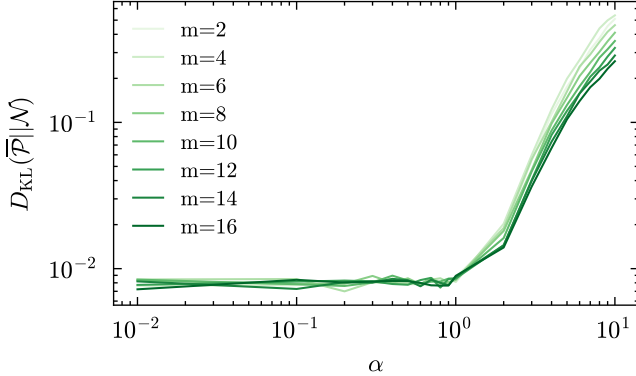


FIG. 7. KL divergence $D(\bar{\mathcal{P}}||\mathcal{N})$ for different α values and number of components m , where $\bar{\mathcal{P}}$ represents the standardized Gaussian mixture distribution.

B. Standardized Gaussian Mixture Results

Second, we investigated the dynamics when the teacher model inputs were standardized, i.e., \mathcal{C} with $\langle\mathcal{C}\rangle = 0$ and $\langle\mathcal{C}^2\rangle^{1/2} = 1$. As before, we first consider $\alpha = 0.001, 0.01, 0.1, 1, 10$ with fixed $\sigma_k = 1$ and $m = 2, 16$ for visualization. Analysis of the dynamics with standardized Gaussian mixtures yielded notable outcomes. As shown in Fig. 5, these mixtures do not introduce any significant discrepancies between ODE dynamics and SGD dynamics.

Further investigation into the KL divergence of standardized Gaussian mixture reveals that this convergence phenomenon is not solely due to the similarity of the distributions. From the previous unstandardized results, we observed that the dynamics approximately converge when the KL divergence is on the order of 10^{-2} . However, as shown by the standardized results in Fig. 7, the KL divergence reaches an order of 10^{-1} in large α scenarios, yet the dynamics under these large α values still exhibit strong convergence. Even for very large α or a regime with large m , the convergence phenomena are maintained.

To examine the effects in a non-homogeneous setting, we set $\alpha = 10$, $\beta = 0.001, 0.01, 0.1, 1, 10$ with $m = 2$ and $m = 16$. As illustrated in Fig. 6, convergence is also observed in the non-homogeneous case. These results suggest that standardization plays a more crucial role in the observed convergence phenomenon. Section V provides an explanation of this phenomenon and why the mixture-based experimental results converge with conventional theory.

V. GEP UNDER STANDARDIZED GAUSSIAN MIXTURES

In this section, we mathematically analyze the convergence properties of the standardized Gaussian mixture. As discussed in Section II, the dynamics of our teacher-student model are governed by the distribution of $\{\lambda, \nu\}$.

To investigate how network dynamics change when C is replaced by a Gaussian mixture \mathcal{C} , it is essential to examine the distribution of $\{\lambda, \nu\}$ in this mixture setting. Since the observed convergence phenomenon occurs exclusively under standardization, for clarity and consistency, we denote \mathcal{C} as its standardized version throughout this section.

Following the proof sequence for the GEP (Property II.3), where $\{\lambda, \nu\}$ obey a joint Gaussian distribution, we extend the proof framework to the Gaussian mixture setting. First, we analyze the distributional property of internal random variables such as λ, ν or U under a Gaussian mixture distribution. Then, we establish the consistency of the preactivation covariance. Since the distribution of $\{\lambda, \nu\}$ dictates the overall dynamics, if the preactivation distribution retains the same in the thermodynamic limit, the dynamics under a standardized Gaussian mixture should also be preserved.

1. Internal Random Variable Gaussianity

In the hidden manifold model dynamics, most updates at each time step do not explicitly involve C or \mathcal{C} in the Gaussian mixture setting. Instead, they are predominantly influenced by $\{\lambda, \nu\}$. The Gaussian nature of preactivations ensures that the dynamics depend only on first- and second-order cumulants. Before analyzing the Gaussianity of preactivations, we first explore the internal random variables λ, ν and U . Consider U defined in matrix form as

$$U = \mathcal{C}F/\sqrt{D} \quad (18)$$

where U has dimensions $\mathbb{R}^{P \times N}$. In practice, we use a dataset of size P , each instance of $U \in \mathbb{R}^{P \times N}$ is generated by sampling P data points. To focus on individual random variables, we consider U in vector form, $U \in \mathbb{R}^N$, where the i -th element is given by

$$U_i = \frac{1}{\sqrt{D}} \sum_{r=1}^D \mathcal{C}_r F_{r,i} \quad (19)$$

with \mathcal{C}_r representing the r -th random variable, drawn from r -th Gaussian mixture. Notice that when generating \mathcal{C} , we sample it from D different Gaussian mixtures. Defining U_i as sum of $A_{r,i}$, we have

$$A_{r,i} = \frac{F_{r,i} \mathcal{C}_r}{\sqrt{D}}, \quad U_i = \sum_{r=1}^D A_{r,i}, \quad s_{D,i}^2 = \frac{1}{D} \sum_{r=1}^D F_{r,i}^2. \quad (20)$$

If the following boundedness assumptions hold, we can apply Lindeberg's condition [38] to establish the central limit theorem for a sequence of independent random variables.

Assumption V.1. There exists $M_{4,\mathcal{C}} \in \mathbb{R}$ such that

$$\sup_{r \geq 1} \mathbb{E}[|\mathcal{C}_r|^4] \leq M_{4,\mathcal{C}} < \infty. \quad (21)$$

Assumption V.2. There exist constants $K_{2,F}, K_{4,F} \in \mathbb{R}$ such that

$$\frac{1}{D} \sum_{r=1}^D F_{r,i}^2 \leq K_{2,F} < \infty, \quad \frac{1}{D} \sum_{r=1}^D F_{r,i}^4 \leq K_{4,F} < \infty. \quad (22)$$

Lindeberg's condition and the corresponding theorem for the independent random variable sequence $A_{r,i}$ are as follows:

Theorem V.3. If a sequence of independent random variables $A_{r,i}$ satisfies Lindeberg's condition

$$\lim_{D \rightarrow \infty} \frac{1}{s_{D,i}^2} \sum_{r=1}^D \mathbb{E} \left[A_{r,i}^2 \mathbf{1}_{\{|A_{r,i}| > \varepsilon s_{D,i}\}} \right] = 0. \quad (23)$$

for all $\varepsilon > 0$, where

$$s_{D,i}^2 := \sum_{r=1}^D \text{Var}(X_{r,i}) = \frac{1}{D} \sum_{r=1}^D F_{r,i}^2. \quad (24)$$

and assuming the variances $\text{Var}(X_{r,i})$ exist and are finite, then

$$U_i \xrightarrow{D \rightarrow \infty} \mathcal{N}(0, s_{D,i}^2) \quad (25)$$

Similarly, we can show that λ_k and ν_m also follow Gaussian distributions under additional boundedness assumptions.

Assumption V.4. There exist constants $K_{2,\widetilde{W}}, K_{4,\widetilde{W}} < \infty$, $K_{2,\widetilde{W}}, K_{4,\widetilde{W}} \in \mathbb{R}$ such that

$$\frac{1}{D} \sum_{r=1}^D \widetilde{W}_{m,r}^2 \leq K_{2,\widetilde{W}}, \quad \frac{1}{N} \sum_{i=1}^N \widetilde{W}_{k,i}^4 \leq K_{4,\widetilde{W}}. \quad (26)$$

Assumption V.5. There exist constants $\delta > 0$, $\exists K_{2,W}, K_{2+\delta,W} < \infty$, $\exists K_{2,W}, K_{2+\delta,W} \in \mathbb{R}$ such that

$$\frac{1}{N} \sum_{i=1}^N W_{k,i}^2 \leq K_{2,W}, \quad \frac{1}{N} \sum_{i=1}^N |W_{k,i}|^{2+\delta} \leq K_{2+\delta,W}. \quad (27)$$

Assumption V.6. There exist $\delta > 0$, $M_{2+\delta} < \infty$, $M_{2+\delta} \in \mathbb{R}$, such that

$$\sup_{i \geq 1} \mathbb{E} \left[|f(U_i) - \mathbb{E}[f(U_i)]|^{2+\delta} \right] \leq M_{2+\delta}. \quad (28)$$

Then, the preactivations individually follow a Gaussian distribution, summarized as follows:

Property V.7. If Assumptions V.1-V.6 hold, the preactivations defined as

$$\lambda_k = \frac{1}{\sqrt{N}} \sum_{i=1}^N W_{k,i} \left(f(U_i) - \mathbb{E}[f(U_i)] \right), \quad (29)$$

$$\nu_m = \frac{1}{\sqrt{D}} \sum_{r=1}^D \mathcal{C}_r \widetilde{W}_{m,r} \quad (30)$$

follows Gaussian distribution in the thermodynamic limit

$$\lambda_k \xrightarrow{N \rightarrow \infty} \mathcal{N}(0, s_{N,k}^2), \quad (31)$$

$$\nu_m \xrightarrow{D \rightarrow \infty} \mathcal{N}(0, \tilde{s}_{D,m}^2), \quad (32)$$

with variances:

$$s_{N,k}^2 = \frac{1}{N} \sum_{i=1}^N W_{k,i}^2 \text{Var}(f(U_i)), \quad (33)$$

$$\tilde{s}_{D,m}^2 = \frac{1}{D} \sum_{r=1}^D \tilde{W}_{m,r}^2 \quad (34)$$

For a detailed derivation of the Gaussianity of preactivations and the verification of assumptions in our setting, refer to Appendix C. Additionally, the Cramér–Wold theorem [39] states that if every linear combination of random variables $a_1 \lambda_1 + a_2 \lambda_2, \dots, a_K \lambda_K$ is Gaussian, then $(\lambda_1, \lambda_2, \dots, \lambda_K)$ follows jointly Gaussian. Since the sum of Gaussian variables remains Gaussian even if they are correlated, we conclude that $\{\lambda, \nu\}$ follows a joint Gaussian distribution.

2. Preactivation Covariance Consistency

Since the preactivations $\{\lambda, \nu\}$ follow a joint Gaussian distribution in the thermodynamic limit, the remaining condition for dynamic convergence is the consistency of covariance. This is because the neural network dynamics depend on the preactivation distribution, and given that the preactivations are jointly Gaussian, ensuring consistency in their mean and covariance is sufficient for maintaining dynamic consistency.

In particular, since the teacher preactivation covariance ($\mathbb{E}[\nu_m \nu_n]$) consistent during training, it remains to show that $\mathbb{E}[\lambda_k \lambda_\ell]$ and $\mathbb{E}[\lambda_k \nu_n]$ have the same asymptotic form as Eq. (10), Eq. (11). The expectation values of preactivation covariance involve terms such as $\mathbb{E}[f(U_i) f(U_j)]$ from Q or $\mathbb{E}[f(U_i) \mathcal{C}_r]$ from R . Goldt *et al.* [1] have utilized function correlation decomposition,

Lemma V.8. *Consider two Gaussian random variables u_1 and u_2 with zero mean, i.e., $\mathbb{E}[u_1] = 0$, $\mathbb{E}[u_2] = 0$, and define their covariances as:*

$$\mathbb{E}[u_1^2] = 1, \quad \mathbb{E}[u_2^2] = 1, \quad \mathbb{E}[u_1 u_2] = \epsilon m. \quad (35)$$

Then, in the $\epsilon \rightarrow 0$ limit:

$$\mathbb{E}[f_1(u_1) f_2(u_2)] = a_1 a_2 + \epsilon m b_1 b_2 + \mathcal{O}(\epsilon^2) \quad (36)$$

where $a_i = \mathbb{E}[u_i]$ and $b_i = \mathbb{E}[u_i f_i(u_i)]$.

In the Gaussian mixture setting, where \mathcal{C}_r is used instead of a simple Gaussian variable, we need to generalize the above lemma. Since a Gaussian mixture is a probabilistic sampling from multiple Gaussian distributions, the following lemma holds naturally:

Lemma V.9. *Given two vector $u_1 \in \mathbb{R}^I$ and $u_2 \in \mathbb{R}^J$ represented as $u_1 = (u_{1,1}, u_{1,2}, \dots, u_{1,I})^\top$ and $u_2 = (u_{2,1}, u_{2,2}, \dots, u_{2,J})^\top$ where each element follows a Gaussian mixture with probability density functions:*

$$p(u_1) = \sum \pi_k \mathcal{N}(\mu_k, \sigma_k^2), \quad p(u_2) = \sum \pi_l \mathcal{N}(\mu_l, \sigma_l^2) \quad (37)$$

where π_k and π_l represent the weights for each component. After standardization to zero mean and unit variance:

$$\mathbb{E}[u_{1,i}] = \mathbb{E}[u_{2,j}] = 0, \quad (38)$$

$$\text{Var}[u_{1,i}] = \text{Var}[u_{2,j}] = 1. \quad (39)$$

Assuming weakly correlated covariance:

$$\mathbb{E}[u_{1,i} u_{2,j}] = \epsilon m_{12}. \quad (40)$$

The function correlation can be decomposed as follows in the limit $\epsilon \rightarrow 0$:

$$\mathbb{E}[f(u_1) g(u_2)] = \sum_{k,l} \pi_k \pi_l \langle f(u_1) \rangle_k \langle g(u_2) \rangle_l + \mathcal{O}(\epsilon) \quad (41)$$

where $\langle \cdot \rangle_k$ represents the expectation with respect to the Gaussian distribution of the k -th component of the mixture.

This result is a straightforward extension of the Gaussian case. For a detailed derivation of expansion, refer to Appendix D. Using this, we can establish that the covariance retains the same asymptotic form as in the GEP II.3.

For example, The definition of R is given by

$$\mathbb{E}[\bar{\lambda}_k \nu_m] = \frac{1}{\sqrt{N}} \sum_{i=1}^N W_{k,i} \frac{1}{\sqrt{D}} \tilde{W}_{m,r} \mathbb{E}[f(U_i) \mathcal{C}_r]. \quad (42)$$

The stochastic dependency arises only through $\mathbb{E}[f(U_i) \mathcal{C}_r]$. Since U_i and \mathcal{C}_r exhibit weak correlation, with $\text{Cov}[U_i \mathcal{C}_r] = F_{r,i} / \sqrt{D}$, the function correlation can be decomposed accordingly. Due to the standardization property of \mathcal{C}_r the resulting expression matches Eq. (11). For a detailed derivation of covariance consistency, refer to Appendix E.

3. Generalized GEP

As a result, our findings can be summarized as a generalized version of the GEP.

Property V.10 (Generalized GEP). *If Assumption II.1, Assumption II.2 and additional Assumptions V.1-V.6 hold, then in the thermodynamic limit $N \rightarrow \infty$ and $D \rightarrow \infty$, regardless of whether C follows a standard Gaussian distribution or a standardized Gaussian mixture ($C \equiv \mathcal{C}$), the preactivations $\{\lambda, \nu\}$ remain jointly Gaussian variables with the same mean and variance as in the original GEP II.3.*

VI. DISCUSSION

In this section, we discuss our results by examining their limitations and potential extensions. First, since a Gaussian mixture with sufficiently many components can approximate arbitrary distributions, we evaluate our findings under various distributional settings. Second, we analyze the error between ODE dynamics and SGD dynamics when the input exhibits correlation beyond the weak correlation assumption. As our derivation applies only under the weak correlation condition, we cannot theoretically quantify this error, but we can investigate it through empirical results.

A. Results from various distribution settings

TABLE I. Parameters for various distributions used in the experiments

Distribution	Parameter(s)
uniform	$a = 0, b = 10$
beta (1)	$\alpha = 0.5, \beta = 0.5$
beta (2)	$\alpha = 5, \beta = 1$
Poisson	$\lambda = 2$
Laplace	$\mu = 0, b = 1$
Pareto	$\alpha = 5$
Lorentz	$x_0 = 0, \gamma = 1$
Gaussian mixture	$p_i = 0.3, 0.7,$ $\mu_i \sim \mathcal{U}[-2, 2], \sigma_i \sim \mathcal{U}[0.5, 5]$

As our mathematical proof shows, the only conditions for dynamics convergence are (1) standardization, and (2) weakly correlation in thermodynamic limit. Therefore, for an arbitrary distribution with standardization, convergence results are expected to be obtained. We consider several distributions that are distinct from simple Gaussian and observe the SGD dynamics. For standardization, we take expectation values from samples to calculate sample mean and sample variance. The distribution parameter information is summarized in Table I.

In Fig. 8, we observe the expected convergence phenomena. Additionally, if we use a distribution that has no low-order cumulant, standardization cannot theoretically align its low-order cumulants with those of a standard Gaussian distribution. To strengthen our discussion through example, we consider the Lorentz distribution, which has no mean or variance. For compact visualization, we use the dynamics of v_k .

In Fig. 9, we see that even standardization cannot make the dynamics converge. This direct example reaffirms that the cumulant property is the key factor for universality.

Ultimately, despite the distinct input distributions deviating from simple Gaussian, standardization and weak correlation that adhere to the Property V.10 lead the dy-

namics of the neural network to asymptotically converge to those anticipated under simple Gaussian inputs.

B. Correlation Effects on Dynamic Behavior

As demonstrated in our analysis, the convergence of dynamics primarily relies on the assumption of *weakly correlation*, where correlations diminish in the thermodynamic limit. This property arises due to our choice of \mathcal{C} and feature matrix F , both of which are sampled i.i.d. from their respective distributions, as well as the teacher and student model weights, which are drawn i.i.d. from a standard Gaussian distribution. In theoretical approaches, assuming uncorrelated random variables is a common choice. For instance, in both the hidden manifold model and the conventional teacher-student model, the teacher model itself is constructed using i.i.d. weights, ensuring no intrinsic correlation with its input. However, in practical applications, correlations naturally emerge. If the teacher model is *informative*, meaning it encodes meaningful structure from the data, correlations between its weights and inputs become inevitable. This trade-off between informativeness and weak correlation poses a challenge in applying the teacher-student framework to real-world scenarios.

Moreover, these correlations do not only arise between teacher model weights and inputs but also among the teacher model weights themselves and among inputs themselves. In this subsection, we empirically investigate this trade-off using real-world data. Since our mathematical justification of convergence in standardized Gaussian mixtures depends on the weak correlation assumption, we cannot theoretically determine how increasing correlation affects dynamics, but we explore this question through empirical analysis.

1. Correlated setting with real-world data

To study weakly to moderately correlated settings and assess applicability to real-world data, we employ an encoder-teacher model framework. In this setup:

- An encoder model is trained to encode the MNIST dataset into a lower-dimensional representation, \mathcal{C} .
- A teacher model receives the standardized version of the encoded output, represent as $\bar{\mathcal{C}}$, and is trained to classify the original MNIST images as odd or even.

Since Gaussian mixtures can approximate arbitrary distributions in the large-component limit, we continue to use the notation \mathcal{C} in this setting. If the encoder-teacher model is well trained, the standardized input $\bar{\mathcal{C}}$ to the teacher model retains compressed information from MNIST, and the teacher model itself contains structured information necessary for classification. Additionally, to

Order parameters dynamics (act: ReLU, nonlinear: sgn)

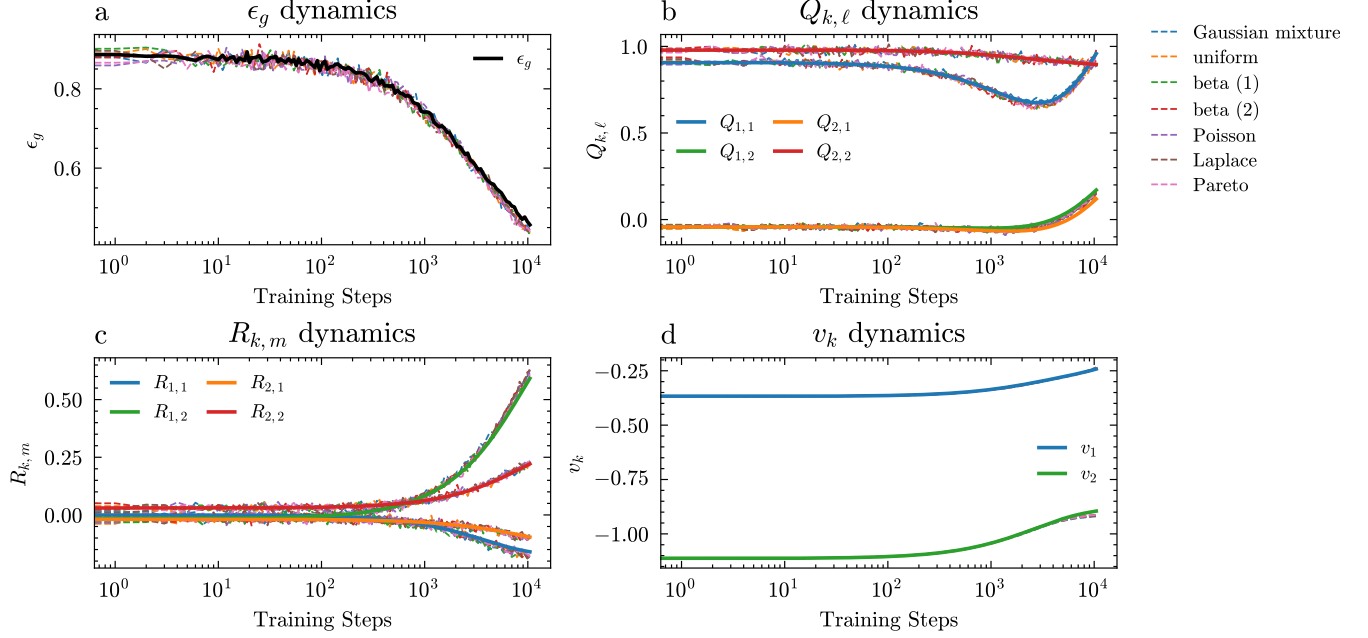


FIG. 8. Examples of dynamics under various distribution settings. Dynamics of (a) generalization error ϵ_g , (b) covariance matrix Q , (c) covariance matrix R , and (d) weight of the second layer v . The SGD results are averaged over 10 runs.

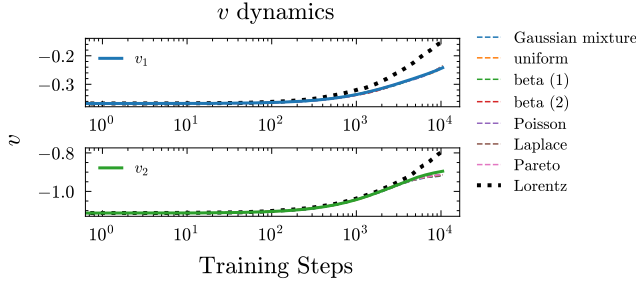


FIG. 9. Example of v_k dynamics under various distribution settings, including the Lorentz distribution.

explicitly control correlation effects, we modify the training objective of the teacher model by incorporating a correlation regularization loss:

$$\mathcal{L} = \lambda_{corr}[\mathcal{L}_{corr,\tilde{W}} + \mathcal{L}_{corr,U} + \mathcal{L}_{corr,v}] + |y - \hat{y}|^2 \quad (43)$$

where

$$\mathcal{L}_{corr,\nu} = |\text{Cov}(\nu_i, \nu_j | \tilde{\mathcal{C}}) - \text{Cov}(\nu_i, \nu_j | \mathcal{C})| \quad (44)$$

$$\mathcal{L}_{corr,U} = |\text{Cov}(U_i, U_j | \tilde{\mathcal{C}}) - \text{Cov}(U_i, U_j | \mathcal{C})| \quad (45)$$

$$\mathcal{L}_{corr,\tilde{W}} = |\text{Cov}(\tilde{W}_i, \tilde{W}_j | \tilde{\mathcal{C}}) - \text{Cov}(\tilde{W}_i, \tilde{W}_j | \mathcal{C})|. \quad (46)$$

Here, $\text{Cov}[a, b | \mathcal{C}]$ represents the covariance of random variables a and b under teacher model input \mathcal{C} , $|\cdot|$ denote element-wise ℓ_1 norm. By adjusting the strength of the correlation loss λ_{corr} , we obtain teacher models and

inputs $\tilde{\mathcal{C}}$ with varying degrees of informativeness and correlation. We train the encoder-teacher model using 10^4 samples from MNIST, reducing the input dimension to $D = 500$, $\mathcal{C} \in \mathbb{R}^D$, significantly lower than the original MNIST dimension 28×28 . Training is performed with full-batch Adam optimization with learning rate 0.001, and we terminate training after 30 epochs. We vary λ_{corr} over the range $[1, 10]$.

2. Empirical causes of dynamic error

Using the trained teacher models and inputs \mathcal{C} , we measure:

- Label accuracy (Acc.), which reflects the degree of informativeness of the teacher model.
- Total correlation loss (\mathcal{L}_{corr}), which quantifies the correlation between internal variables.
- Dynamic error ($e_{\mathcal{D}}$), which measures the discrepancy between ODE and SGD dynamics:

$$e_{\mathcal{D}} = \|\mathcal{D}_{\text{SGD}}(\tau) - \mathcal{D}_{\text{ODE}}(\tau)\|_2 \quad (47)$$

where \mathcal{D} represents variables such as ϵ_g , $Q_{k,\ell}$, $R_{k,m}$ or v_k , and $\tau = 1000$ denotes the evaluation time step. The ℓ_2 norm $\|\cdot\|_2$ quantifies the error magnitude. Since SGD updates introduce randomness due to sample selection, we compute $e_{\mathcal{D}}$ by averaging over 20 runs of SGD with a fixed student model. We also evaluate the accuracy

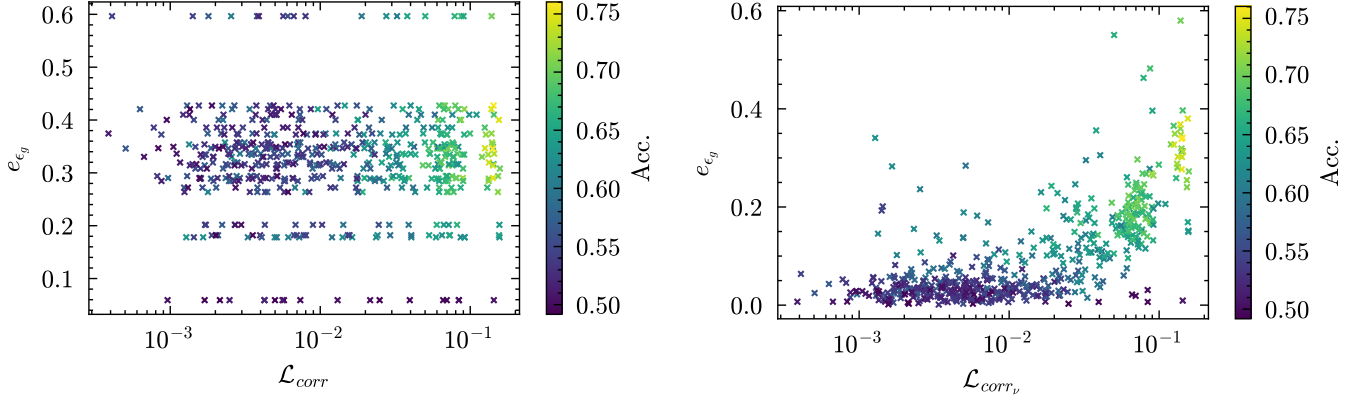


FIG. 10. Left panel: Relationship between total correlation loss \mathcal{L}_{corr} (x-axis) and dynamic error e_{ϵ_g} (y-axis). The color represents classification accuracy on the training dataset, and each point corresponds to a specific teacher model and teacher model input pair obtained from the encoder-teacher training process. Right panel: The same plot, but with the x-axis replaced by $\mathcal{L}_{corr, \nu}$, isolating the correlation effect of ν .

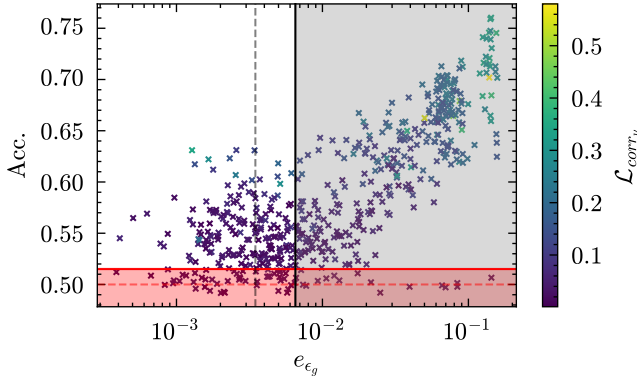


FIG. 11. Revised visualization highlighting the relationship among dynamic error e_{ϵ_g} (x-axis), accuracy (y-axis) and $\mathcal{L}_{corr, \nu}$ (color). The red dotted and solid horizontal lines indicate the mean accuracy, 0.5 and $0.5 + 3\sigma_{acc}$ of a random classifier, respectively. The black dotted and solid lines represent the empirical stochastic error magnitude, calculated as the mean e_{ϵ_g} , e_{base} and $e_{base} + \sigma_{base}$, respectively.

using training samples 10^4 . As each dynamic variable is updated proportional to the magnitude of each timestep error, which relate to ϵ_g , we mainly focus on ϵ_g as a dynamic quantity \mathcal{D} .

Fig. 10 illustrates the relationships among correlation loss, accuracy, and dynamic error. As correlation loss increases, accuracy also increases, exhibiting a strong correlation. This aligns with our expectation that more informative models deviate further from weakly correlated dynamics. The Pearson correlation coefficients ρ confirm this trend, given by $\rho(\text{Acc.}, e_{\epsilon_g}) = 0.774$. However, we do not observe a direct correlation between total correlation loss \mathcal{L}_{corr} and dynamic error e_{ϵ_g} or between \mathcal{L}_{corr} and accuracy. To investigate further, we decompose the correlation loss into its components: $\mathcal{L}_{corr, \nu}$,

$\mathcal{L}_{corr, U}$, and $\mathcal{L}_{corr, \tilde{W}}$. Unlike $\mathcal{L}_{corr, U}$ and $\mathcal{L}_{corr, \tilde{W}}$, which have weak correlation with accuracy, we find that $\mathcal{L}_{corr, U}$ strongly correlates with both accuracy and dynamic error. In Fig. 10, the right panel directly show strong correlation among correlation loss, accuracy, and average dynamics error. A high correlation loss corresponds to high accuracy with a large dynamic error, whereas a small correlation loss corresponds to low accuracy and a small dynamic error, and vice versa. The Pearson correlation coefficients ρ among these variables are given by $\rho(\mathcal{L}_{corr, \nu}, \text{Acc}) = 0.833$, $\rho(\mathcal{L}_{corr, \nu}, e_{\epsilon_g}) = 0.762$, and $\rho(e_{\epsilon_g}, \text{Acc}) = 0.774$. From these observations, we hypothesize that ‘the correlation between teacher model inputs $\bar{\mathcal{C}}$ and teacher model weights \tilde{W} plays a crucial role in dynamic consistency.’ Theoretically, since our proofs assume weak correlation, we cannot rigorously quantify its detailed effect. However, empirically, we show correlation between teacher model and teacher model input appears to be the dominant factor.

3. Possible extensions in correlated scenarios

Given the trade-off between correlation strength and model informativeness, we now consider whether our theoretical approach can still provide insights for real-world applications. To test this, we construct the hypothesis: “We cannot track the dynamics of an informative model.” To refute this hypothesis, we must show that even for informative models, dynamic tracking remains feasible. First, a non-informative model can be approximated as a random classifier, which has a 50% chance of correct classification. Given n samples, the probability of correctly labeling k samples follows a binomial distribution, leading to an accuracy variance of $\sigma_{acc} = 1/(2\sqrt{n})$. For our case $n = 10^4$, a model achieving accuracy above $0.5 + 3\sigma_{acc}$ can be considered informative with high confidence. Second, we assess whether we can track dynam-

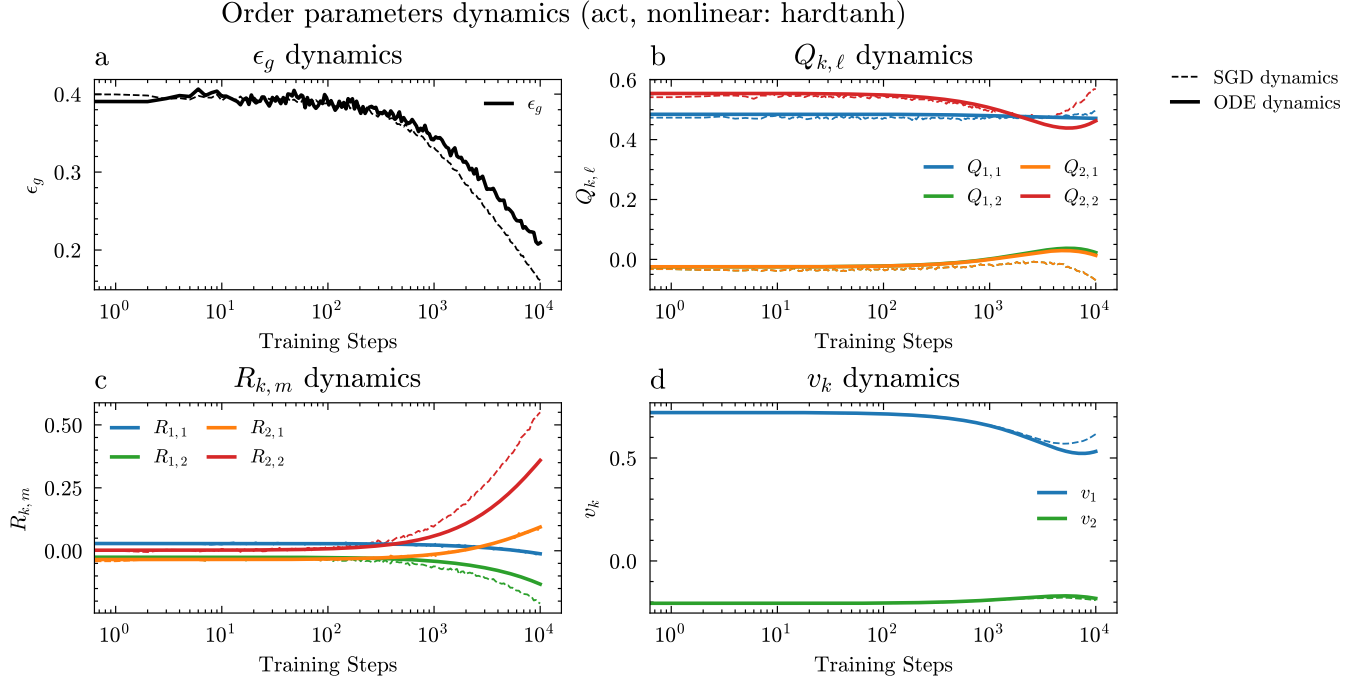


FIG. 12. Example dynamics for selected teacher model and teacher model input. Dynamics of (a) generalization error ϵ_g , (b) covariance matrix Q , (c) covariance matrix R , and (d) weight of the second layer v . The SGD results are averaged over 5 runs.

ics under moderate correlation. Even when the teacher model input is Gaussian, stochastic error in SGD introduces a baseline error between SGD and ODE dynamics. We denote the mean and standard deviation of this baseline error as e_{base} and σ_{base} . If the dynamic error from a non-Gaussian input \mathcal{C} remains within $e_{\text{base}} + \sigma_{\text{base}}$, we conclude that tracking is feasible to some extent. So, we calculate mean and variance from 20 individual SGD dynamics under same initial conditions (fixed teacher, student model and feature matrix F).

Fig. 11 visualizes relation between accuracy and dynamic error, with thresholds for informativeness ($0.5 + 3\sigma_{\text{acc}}$) and tracking feasibility ($e_{\text{base}} + \sigma_{\text{base}}$). The first quadrant represents teacher model and input pair region that are both informative and trackable, indicating that despite existence of moderate correlations, approximate trends can still be captured. This suggests that while our framework may not be directly applicable in all practical settings, it remains useful in scenarios where correlations are numerically weak, allowing for approximate tracking of dynamic behavior.

As an example, Fig. 12 presents a trajectory for an informative model that falls in the first quadrant. Even beyond our evaluation timestep $\tau = 1000$, the observed dynamics provide feasible results.

VII. CONCLUSION

Previous studies have examined the dynamics of neural networks under simple Gaussian distributions and Gaus-

sian mixtures without hidden manifolds [1, 19, 20, 40–42]. Our work extends this by investigating dynamics with Gaussian mixtures in a manifold setting. We compared dynamics under simple Gaussian inputs to those under Gaussian mixture inputs using SGD, identifying key differences.

The key takeaway from our study is the pivotal role of standardization and weak correlation condition in dynamics. Standardization ensures that any input distribution has identical second-order cumulants to a normal Gaussian, while the weak correlation condition, combined with bounded assumptions, allows internal random variables to behave as Gaussians via the central limit theorem. This Gaussianity simplifying their mathematical treatment and analysis. In essence, our findings suggest a form of universality in neural network dynamics.

Additionally, numerical experiments using a real dataset, where the teacher model input is structured rather than purely random, provided empirical insights into the role of correlation in convergence. By analyzing various teacher model and input pairs, we demonstrated the potential applicability of our framework in capturing real-world scenarios to some extent. Future work could extend this framework by applying the findings to more complex, real-world datasets and relaxing some of the stricter assumptions.

Exploring how deep learning parameters behave can be key to understanding the generalization ability of deep learning. We expect that our research will contribute to bridging the gap between the practical successes of applied deep learning and its developing theoretical foun-

dations.

VIII. REPRODUCIBILITY

For a comprehensive understanding of our numerical SGD implementation and ODE update mechanisms and to ensure reproducibility, please visit our code repository at <https://github.com/peardragon/GaussianUniversality>.

ACKNOWLEDGMENTS

This study was supported by the Basic Science Research Program through the National Research Foundation of Korea (RS-2025-00514776).

Appendix A: Derivation of Gaussian Equivalent Property and ODE

This appendix section rephrases the research from Goldt *et al.* [1] to align with the notation used in the main script. For match the subscripts of manuscripts, original super(sub)scripts are reorganized.

1. Correlation of Two Functions

It is important to consider how to express the correlation of functions, such as $\mathbb{E}[f(x)g(y)]$, for the analysis of neural network dynamics. Let's consider random variables following a $\mathcal{N}(0, 1)$ distribution and examine the correlation of functions taking these random variables as inputs.

Represent two random variables, adhering to a joint Gaussian distribution, as vectors,

$$x = (x_1, \dots, x_I)^\top, \quad y = (y_1, \dots, y_J)^\top. \quad (\text{A1})$$

The assumption of joint Gaussian distribution for these random variables implies that the vectors have the fol-

lowing mean and covariance.

$$\begin{aligned} \mathbb{E}[x_i] &= \mathbb{E}[y_j] = 0, \\ \mathbb{E}[x_i x_j] &= Q_{ij}, \quad \mathbb{E}[y_i y_j] = R_{ij}, \quad \mathbb{E}[x_i y_j] = \epsilon S_{ij} \end{aligned} \quad (\text{A2})$$

The joint distribution of x and y can be represented as:

$$P = \frac{1}{Z} \exp \left[-\frac{1}{2} \begin{pmatrix} x & y \end{pmatrix} \begin{pmatrix} Q & \epsilon S \\ \epsilon S^\top & R \end{pmatrix}^{-1} \begin{pmatrix} x \\ y \end{pmatrix} \right] \quad (\text{A3})$$

Considering a first-order approximation in ϵ , the inverse matrix part becomes,

$$\begin{pmatrix} Q & \epsilon S \\ \epsilon S^\top & R \end{pmatrix}^{-1} = \begin{pmatrix} Q & 0 \\ 0 & R \end{pmatrix}^{-1} - \epsilon M + \mathcal{O}(\epsilon^2) \quad (\text{A4})$$

where

$$M = \begin{pmatrix} 0 & Q^{-1} S R^{-1} \\ [Q^{-1} S R^{-1}]^\top & 0 \end{pmatrix}. \quad (\text{A5})$$

Inserting this back into the joint distribution and approximating again with respect to ϵ , we obtain following results.

$$P(x, y) = \frac{1}{Z} \exp [A + B] \quad (\text{A6})$$

where

$$A = -\frac{1}{2} \begin{pmatrix} x & y \end{pmatrix} \begin{pmatrix} Q^{-1} & 0 \\ 0 & R^{-1} \end{pmatrix} \begin{pmatrix} x \\ y \end{pmatrix} \quad (\text{A7})$$

and

$$B = 1 + \epsilon \sum_{i=1}^I \sum_{j=1}^J x_i (Q^{-1} S R^{-1})_{ij} y_j + \mathcal{O}(\epsilon^2). \quad (\text{A8})$$

To directly apply the aforementioned equation to the correlation of two functions, consider $f(x)$ and $g(y)$ as functions of x and y , respectively. Provided these functions are sufficiently regular to possess expectations $\mathbb{E}_x[x_i f(x)]$, $\mathbb{E}_y[y_j g(y)]$, $\mathbb{E}_x[x_i x_j f(x)]$, and $\mathbb{E}_y[y_i y_j g(y)]$, the correlation between the two functions $\mathbb{E}[f(x)g(y)]$ can be expressed as:

$$\mathbb{E}[f(x)g(y)] = \mathbb{E}[f(x)]\mathbb{E}[g(y)] + \epsilon \sum_{i=1}^I \sum_{j=1}^J \mathbb{E}[x_i f(x)](Q^{-1} S R^{-1})_{ij} \mathbb{E}[y_j g(y)] + \mathcal{O}(\epsilon^2), \quad (\text{A9})$$

as derived by [1].

2. Gaussian Equivalence Property

From the function correlation approximations, it becomes clear that for functions of sufficient regularity,

their correlations are primarily dictated by the function's mean, distribution characteristics such as $\mathbb{E}[uf(u)]$, and the covariance of the original random variables. This underscores the pivotal role of function correlation in dissecting the dynamics within neural networks. We summarized previous results derived by Goldt *et al.* [1].

In our investigation, the weight update mechanism is facilitated by employing a straightforward stochastic gradient descent (SGD) strategy, with the batch size set to one.

$$W_{k,i} := W_{k,i} - \frac{\eta}{\sqrt{N}} v_k (\hat{y} - y) g'(\lambda_k) f(U_i) \quad (\text{A10})$$

$$v_k := v_k - \frac{\eta}{N} g(\lambda_k) (\hat{y} - y) \quad (\text{A11})$$

By defining the normalized number of steps as $t = 1/N$ within the thermodynamic limit as $N \rightarrow \infty$, which analogously functions as a continuous time-like variable, we are equipped to elucidate the dynamics of the second layer weight in the student model by examining the function correlations of the preactivations from an averaged standpoint. Consequently, the dynamics of v_k adhere to the following ODE formulation.

$$\frac{dv_k}{dt} = \eta \left[\sum_n^M \tilde{v}_n I_1 - \sum_j^K v_j I_2 \right] \quad (\text{A12})$$

where

$$I_1 = \mathbb{E}[g(\lambda_k) \tilde{g}(\nu_n)], \quad I_2 = \mathbb{E}[g(\lambda_k) g(\lambda_j)]. \quad (\text{A13})$$

Given the crucial role of function correlation in unpacking the dynamics prompted by weight updates, it is imperative to understand the distribution characterizing λ, ν to compute expectation values such as $\mathbb{E}[g(\lambda_k) \tilde{g}(\nu_n)]$. This analytical approach enables a deeper understanding of the underlying mechanics governing the behavior of neural networks, particularly in how weight adjustments influence overall learning and adaptation processes.

Unlike the earlier discussion on simple function correlation, where the variable x of the function was assumed to be a simple Gaussian, in the context of deep learning SGD updates, the random variable entering the function is not just an assumable random variable but the preactivations.

Therefore, it's essential to ascertain the distribution of these preactivations. We need to starting following assumptions, Assumption II.1 and Assumption II.2, taken from Goldt *et al.* [1].

In typical deep learning scenarios, activations that address gradient vanishing or explosiveness involve gradients directly influencing weight updates in a non-vanishing limit. Thus, considering bounds for student weights during initialization is sufficient. Since the remaining teacher weights and feature matrix F are constant, ensuring proper bounds for teacher and student weights during initialization, and setting the feature matrix F to be sufficiently bounded, these assumptions can be adequately met.

With these assumptions and the result of function correlation, the Gaussian Equivalence Property holds as follows:

Property A.1 (Gaussian Equivalence Property (GEP)). *In the thermodynamic limit ($N \rightarrow \infty$, $D \rightarrow \infty$), with finite K , M , D/N , and under the Assumption ?? and Assumption ??, if the C follows a normal Gaussian distribution $\mathcal{N}(0, I)$, then $\{\lambda, \nu\}$ conform to $K + M$ jointly Gaussian variables. This means that statistics involving $\{\lambda, \nu\}$ are entirely represented by their mean and covariance.*

This property derived by Goldt *et al.* [1] allows us to representing characteristics of the student and teacher models, generalization error and dynamics of the student model's second layer weights, through the mean and covariance of the joint Gaussian distribution of preactivations.

For convenience, let's redefine $\bar{\lambda}_k$ as:

$$\bar{\lambda}_k = \frac{1}{\sqrt{N}} \sum_{i=1}^N W_{k,i} (f(U_i) - \mathbb{E}_{u \sim \mathcal{N}(0,1)}[f(u)]) \quad (\text{A14})$$

$\bar{\lambda}_k$ also follows a jointly Gaussian distribution, and its expectation value satisfies $\mathbb{E}[\bar{\lambda}_k] = 0$ as per function correlation.

In this appendix, we present a concise derivation of $Q_{k,\ell}$. For a additional derivation, we refer the reader to prior research [19]. To facilitate the explanation, we first define a , b , and c as statistical properties of the nonlinear function f , which is utilized in transforming the student model inputs X , where $X = f(CF/\sqrt{D})$:

$$\begin{aligned} a &= \mathbb{E}_{u \sim \mathcal{N}(0,1)}[f(u)], \\ b &= \mathbb{E}_{u \sim \mathcal{N}(0,1)}[uf(u)], \\ c &= \mathbb{E}_{u \sim \mathcal{N}(0,1)}[f(u)^2] \end{aligned} \quad (\text{A15})$$

With these definitions in place, $Q_{k,\ell}$ can be expressed as follows:

$$\begin{aligned} Q_{k,\ell} &\equiv \mathbb{E}[\bar{\lambda}_k \bar{\lambda}_\ell] \\ &= \mathbb{E}\left[\frac{1}{N} \sum_{i=1}^N \sum_{j=1}^N W_{k,i} W_{\ell,j} (f(U_i) - a)(f(U_j) - a)\right] \end{aligned} \quad (\text{A16})$$

Considering the case where $i \neq j$, and applying the expectation, we implement the function correlation approximation A9 to derive:

$$\mathbb{E}[f(U_i) f(U_j)] = a^2 + \frac{1}{D} \sum_{r=1}^D F_{r,i} F_{r,j} b^2 \quad (\text{A17})$$

in thermodynamic limit or

$$\mathbb{E}[(f(U_i) - a)(f(U_j) - a)] = \frac{1}{D} \sum_{r=1}^D F_{r,i} F_{r,j} b^2. \quad (\text{A18})$$

Hence, $Q_{k,\ell}$ can be succinctly rearranged for both $i \neq j$ and $i = j$ cases as:

$$Q_{k,\ell} = (c - a^2) \frac{1}{N} \sum_{i=j=1}^N W_{k,i} W_{\ell,j} + \frac{1}{N} \sum_{i \neq j}^N W_{k,i} W_{\ell,j} [b^2 \frac{1}{D} \sum_{r=1}^D F_{r,i} F_{r,j}] \quad (\text{A19})$$

$$= (c - a^2 - b^2) \frac{1}{N} \sum_{i=j=1}^N W_{k,i} W_{\ell,j} + \frac{1}{N} \sum_{i,j}^N W_{k,i} W_{\ell,j} [b^2 \frac{1}{D} \sum_{r=1}^D F_{r,i} F_{r,j}] \quad (\text{A20})$$

A similar approach can be applied to derive the remaining covariance components. Regarding high-order moments, an analogous method is employed by extending the function correlation approximation results, Eq. (A9) to more general cases, thereby demonstrating that such preactivations follow a Gaussian distribution in the thermodynamic limit. For a comprehensive explanation of this process, the reader is encouraged to consult the referenced research [1].

Consequently, the new distribution $\{\bar{\lambda}, \nu\}$ follows a more straightforward distribution with the mean

$$\mathbb{E}[\bar{\lambda}_k] = \mathbb{E}[\nu_m] = 0 \quad (\text{A21})$$

and the covariance

$$Q_{k,\ell} \equiv \mathbb{E}[\bar{\lambda}_k \bar{\lambda}_\ell] = (c - a^2 - b^2) \Omega_{k,\ell} + b^2 \Sigma_{k,\ell} \quad (\text{A22})$$

$$R_{k,m} \equiv \mathbb{E}[\bar{\lambda}_k \nu_m] = b \frac{1}{D} \sum_{r=1}^D S_{k,r} \widetilde{W}_{m,r} \quad (\text{A23})$$

$$T_{m,n} \equiv \mathbb{E}[\nu_m \nu_n] = \frac{1}{D} \sum_{r=1}^D \widetilde{W}_{m,r} \widetilde{W}_{n,r}. \quad (\text{A24})$$

The newly defined matrices satisfy the following rela-

tions:

$$S_{k,r} \equiv \frac{1}{\sqrt{N}} \sum_{i=1}^N W_{k,i} F_{r,i}, \quad (\text{A25})$$

$$\Omega_{k,\ell} \equiv \frac{1}{N} \sum_{i=1}^N W_{k,i} W_{\ell,i}, \quad (\text{A26})$$

$$\Sigma_{k,\ell} \equiv \frac{1}{D} \sum_{r=1}^D S_{k,r} S_{\ell,r}, \quad (\text{A27})$$

3. Derivation of the ODE for Covariance and Weights

To derive the ODE for our main metrics of interest - the covariances Q , R , and the second layer weight v - we begin with our single batch gradient update.

$$W_{k,i} := W_{k,i} - \frac{\eta}{\sqrt{N}} v_k (\hat{y} - y) g'(\lambda_k) f(U_i), \quad (\text{A28})$$

$$v_k := v_k - \frac{\eta}{N} g(\lambda_k) (\hat{y} - y) \quad (\text{A29})$$

The preactivations are related to the first layer weights, and thus we consider quantities such as $S_{k,r}$ and $\Sigma_{k,\ell}$ that are proportional to the first layer weights W . The dynamics of the first layer weights are determined by a term involving $(\hat{y} - y) g'(\lambda_k) f(U_i)$, assuming the second layer is constant. The average update of these quantities can be obtained from the following equation:

$$\left[\sum_{j=1}^K v_j g(\lambda_j) - \sum_{m=1}^M \tilde{v}_m \tilde{g}(v_m) \right] g'(\lambda_k) f(U_i) \quad (\text{A30})$$

Starting with $S_{k,r} \equiv \frac{1}{\sqrt{N}} \sum_{i=1}^N W_{k,i} F_{r,i}$, we obtain:

$$S_{k,r} := S_{k,r} - \frac{\eta}{\sqrt{N}} v^k \left[\sum_{j \neq k}^K v_j \mathbb{E}[g(\lambda_j) g'(\lambda_k) \beta_r] + v_k \mathbb{E}[g(\lambda_k) g'(\lambda_k) \beta_r] - \sum_n^M \tilde{v}_n \mathbb{E}[\tilde{g}(\nu_n) g'(\lambda_k) \beta_r] \right] \quad (\text{A31})$$

with $\beta_r = \frac{1}{\sqrt{N}} \sum_i F_{r,i} f(U_i)$.

Function correlations are employed to express these

updates in terms of statistical quantities of the distributions λ, ν . However, the equations for covariances remain coupled. To uncouple them, we need to consider the

eigenvectors and eigenvalues, ψ_τ and ρ_τ , of the $D \times D$ matrix \mathcal{F} formed by $\mathcal{F}_{r,s} = 1/N \sum_i F_{r,i} F_{s,i}$. The eigenvectors and eigenvalues are obtained under the following normalization condition:

$$\begin{aligned} \sum_s \mathcal{F}_{r,s} (\psi_\tau)_s &= \rho_\tau (\psi_\tau)_r, \\ \sum_s (\psi_\tau)_s (\psi_{\tau'})_s &= D \delta(\tau, \tau'), \\ \sum_\tau (\psi_\tau)_r (\psi_\tau)_s &= D \delta(r, s) \end{aligned} \quad (\text{A32})$$

Using these, we can express the teacher-student overlap

covariance $R_{k,m}$ through two projected matrices:

$$\mathcal{S}_{k,r} = \frac{1}{\sqrt{D}} \sum_r S_{k,r} (\psi_\tau)_r, \quad \mathcal{W}_{m,\tau} = \frac{1}{\sqrt{D}} \sum_r \widetilde{W}_{m,r} (\psi_\tau)_r \quad (\text{A33})$$

and thus:

$$R_{k,m} = \frac{b}{D} \sum_\tau \mathcal{S}_{k,r} \mathcal{W}_{m,\tau} \quad (\text{A34})$$

Since the teacher model's matrix is static, its projection matrix \mathcal{S} is given by:

$$\mathcal{S}_{k,\tau} := \mathcal{S}_{k,\tau} - \frac{\eta}{\sqrt{DN}} v^k \sum_r (\psi_\tau)_r \left[\sum_{j \neq k}^K v_j \mathbb{E}[g(\lambda_j) g'(\lambda_k) \beta_r] + v_k \mathbb{E}[g(\lambda_k) g'(\lambda_k) \beta_r] - \sum_n^M \tilde{v}_n \mathbb{E}[\tilde{g}(\nu_n) g'(\lambda_k) \beta_r] \right] \quad (\text{A35})$$

The update rule for R is then derived using these projections. Explicitly at timestep t , it can be expressed as:

$$(R_{k,m})_{t+1} - (R_{k,m})_t = \frac{b}{D} \sum_\tau [(\mathcal{S}_{k,\tau})_{t+1} - (\mathcal{S}_{k,\tau})_t] \widetilde{W}_{m,r} \quad (\text{A36})$$

as derived by Goldt *et al.* [1]. During the summation over τ , two types of terms emerge:

$$\mathcal{T}_{m,n} \equiv \frac{1}{D} \sum_\tau \rho_\tau \widetilde{W}_{m,r} \widetilde{W}_{n,r}, \quad \frac{1}{D} \sum_\tau \rho_\tau \mathcal{S}_{\ell,\tau} \widetilde{W}_{n,\tau} \quad (\text{A37})$$

The second summation is not readily reducible to a simpler expression. Instead, we introduce the following density function:

$$r_{k,m}(\rho) = \frac{1}{\epsilon_\rho} \frac{1}{D} \sum_\tau \tilde{S}_{k,\tau} \widetilde{W}_{m,\tau} \mathbf{1}_{\rho_\tau \in [\rho, \rho + \epsilon_\rho]} \quad (\text{A38})$$

This density function allows us to express the covariance

R in terms of the eigenvalue distribution ρ :

$$R_{k,m} = b \int d\rho p(\rho) r_{k,m}(\rho) \quad (\text{A39})$$

Under the assumption that the feature matrix elements are i.i.d. from a normal distribution $\mathcal{N}(0, 1)$, this distribution adheres to the Marchenko-Pastur law [43]:

$$p(\rho) = \frac{1}{2\pi D/N} \frac{\sqrt{((1 + \sqrt{D/N})^2 - \rho)(\rho - (1 - \sqrt{D/N})^2)}}{\rho} \quad (\text{A40})$$

where The update equation for $r_{k,m}(\rho)$ is straightforwardly derived from the update equation and definition of \mathcal{S} . Ultimately, in the thermodynamic limit, with $t = 1/N$ transforming into a continuous time-like variable, the equation of motion for $r_{k,m}(\rho, t)$ satisfies the following ODE:

$$\begin{aligned} \frac{\partial r_{k,m}(\rho, t)}{\partial t} &= -\frac{\eta}{D/N} v_k d(\rho) \left(r_{km}(\rho) \sum_{j \neq k}^K v_j \frac{Q_{jj} \mathbb{E}[g'(\lambda_k) \lambda_k g(\lambda_j)] - Q_{kj} \mathbb{E}[g'(\lambda_k) \lambda_j g(\lambda_j)]}{Q_{jj} Q_{kk} - (Q_{kj})^2} \right. \\ &\quad + \sum_{j \neq k}^K v_j r_{jm}(\rho) \frac{Q_{kk} \mathbb{E}[g'(\lambda_k) \lambda_j g(\lambda_j)] - Q_{kj} \mathbb{E}[g'(\lambda_k) \lambda_k g(\lambda_j)]}{Q_{jj} Q_{kk} - (Q_{kj})^2} \\ &\quad + v_k r_{km}(\rho) \frac{1}{Q_{kk}} \mathbb{E}[g'(\lambda_k) \lambda_k g(\lambda_k)] - \\ &\quad r_{km}(\rho) \sum_n^M \tilde{v}_n \frac{T_{nn} \mathbb{E}[g'(\lambda_k) \lambda_k \tilde{g}(\nu_n)] - R_{kn} \mathbb{E}[g'(\lambda_k) \nu_n \tilde{g}(\nu_n)]}{Q_{kk} T_{nn} - (R_{kn})^2} \\ &\quad \left. - \frac{b\rho}{d(\rho)} \sum_n^M \tilde{v}_n \mathcal{T}_{nm} \frac{Q_{kk} \mathbb{E}[g'(\lambda_k) \nu_n \tilde{g}(\nu_n)] - R_{kn} \mathbb{E}[g'(\lambda_k) \lambda_k \tilde{g}(\nu_n)]}{Q_{kk} T_{nn} - (R_{kn})^2} \right) \end{aligned} \quad (\text{A41})$$

where $d(\rho) = (c-b^2)\frac{D}{N} + b^2\rho$ as derived by Goldt *et al.* [1]. Note that all explicit time dependencies on the right side of the equation are omitted for clarity. In this numerical ODE implementation, the right side corresponds to the immediate preceding time t , and the left side to the updated time $t + 1$.

Similarly, the covariance Q associated with the first weight W can be derived in a repetitive manner, starting from:

$$Q_{k,\ell} \equiv \mathbb{E}[\lambda_k \lambda_\ell] = [c - b^2]W_{k,\ell} + b^2\Sigma_{k,\ell} \quad (\text{A42})$$

Notice that we ignore a term since we focus on symmetric nonlinear function f . Following a similar process as before, we find that the first term, $W_{k,\ell}$, adheres to:

$$\begin{aligned} \frac{dW_{k,\ell}(t)}{dt} = & -\eta v_k \left(\sum_j^K v_j \mathbb{E}[g'(\lambda_k) \lambda_\ell g(\lambda_j)] - \sum_n \tilde{v}_n \mathbb{E}[g'(\lambda_k) \lambda_\ell \tilde{g}(\nu_n)] \right) \\ & - \eta v_\ell \left(\sum_j^K v_j \mathbb{E}[g'(\lambda_\ell) \lambda_k g(\lambda_j)] - \sum_n \tilde{v}_n \mathbb{E}[g'(\lambda_\ell) \lambda_k \tilde{g}(\nu_n)] \right) \\ & + c\eta^2 v_k v_\ell \left(\sum_{j,\ell}^K v_j v_\ell \mathbb{E}[g'(\lambda_k) g'(\lambda_\ell) g(\lambda_j) g(\lambda_\ell)] \right. \\ & - 2 \sum_j^K \sum_m^M v_j \tilde{v}_m \mathbb{E}[g'(\lambda_k) g'(\lambda_\ell) g(\lambda_j) \tilde{g}(\nu_m)] \\ & \left. + \sum_{n,m}^M \tilde{v}_n \tilde{v}_m \mathbb{E}[g'(\lambda_k) g'(\lambda_\ell) \tilde{g}(\nu_n) \tilde{g}(\nu_m)] \right) \end{aligned} \quad (\text{A43})$$

as derived by Goldt *et al.* [1]. The second term, $\Sigma_{k,\ell}$, can be expressed using the rotating basis ψ_τ :

$$\Sigma_{k,\ell} \equiv \frac{1}{D} \sum_r S_{k,r} S_{\ell,r} = \frac{1}{D} \sum_\tau \mathcal{S}_{k,\tau} \mathcal{S}_{\ell,\tau} \quad (\text{A44})$$

and thus, integral form for $\Sigma_{k,\ell}(t)$ can be derived:

$$\sigma_{k,\ell}(\rho) = \frac{1}{\epsilon_\rho} \frac{1}{D} \sum_\tau \mathcal{S}_{k,\tau} \mathcal{S}_{\ell,\tau} \mathbf{1}_{\rho_\tau \in [\rho, \rho + \epsilon_\rho]} \quad (\text{A45})$$

with

$$\begin{aligned}
\frac{\partial \sigma_{k\ell}(\rho, t)}{\partial t} = & -\frac{\eta}{D/N} \left(d(\rho) v_k \sigma_{k\ell}(\rho) \sum_{j \neq k} v_j \frac{Q_{jj} \mathbb{E}[g'(\lambda_k) \lambda_k g(\lambda_j)] - Q_{kj} \mathbb{E}[g'(\lambda_k) \lambda_j g(\lambda_j)]}{Q_{jj} Q_{kk} - (Q_{kj})^2} \right. \\
& + v_k \sum_{j \neq k} v_j d(\rho) \sigma_{j\ell}(\rho) \frac{Q_{kk} \mathbb{E}[g'(\lambda_k) \lambda_j g(\lambda_j)] - Q_{kj} \mathbb{E}[g'(\lambda_k) \lambda_k g(\lambda_j)]}{Q_{jj} Q_{kk} - (Q_{kj})^2} \\
& + d(\rho) v_k \sigma_{k\ell}(\rho) v_k \frac{1}{Q_{kk}} \mathbb{E}[g'(\lambda_k) \lambda_k g(\lambda_k)] \\
& - d(\rho) v_k \sigma_{k\ell}(\rho) \sum_n \tilde{v}_n \frac{T_{nn} \mathbb{E}[g'(\lambda_k) \lambda_k \tilde{g}(\nu_n)] - R_{kn} \mathbb{E}[g'(\lambda_k) \nu_n \tilde{g}(\nu_n)]}{Q_{kk} T_{nn} - (R_{kn})^2} \\
& - b \rho v_k \sum_n \tilde{v}_n r_{\ell n}(\rho) \frac{Q_{kk} \mathbb{E}[g'(\lambda_k) \nu_n \tilde{g}(\nu_n)] - R_{kn} \mathbb{E}[g'(\lambda_k) \lambda_k \tilde{g}(\nu_n)]}{Q_{kk} T_{nn} - (R_{kn})^2} \\
& + \text{all of the above with } \ell \rightarrow k, k \rightarrow \ell). \\
& + \eta^2 v_k v_\ell \left[(c - b^2) \rho + \frac{b^2}{\delta} \rho^2 \right] \left(\sum_{j, \ell}^K v_j v_\ell \mathbb{E}[g'(\lambda_k) g'(\lambda_\ell) g(\lambda_j) g(\lambda_\ell)] \right. \\
& \left. - 2 \sum_j^K \sum_m^M v_j \tilde{v}_m \mathbb{E}[g'(\lambda_k) g'(\lambda_\ell) g(\lambda_j) \tilde{g}(\nu_m)] + \sum_{n, m}^M \tilde{v}_n \tilde{v}_m \mathbb{E}[g'(\lambda_k) g'(\lambda_\ell) \tilde{g}(\nu_n) \tilde{g}(\nu_m)] \right)
\end{aligned} \tag{A46}$$

as derived by Goldt *et al.* [1]. The weight v and generalization error ϵ_g can be directly obtained from the weight update formula and the definition of generalization error

with MSE:

$$\frac{dv_k}{dt} = \eta \left[\sum_n^M \tilde{v}_n \mathbb{E}[g(\lambda_k) \tilde{g}(\nu_n)] - \sum_j^K v_j \mathbb{E}[g(\lambda_k) g(\lambda_j)] \right] \tag{A47}$$

with

$$\begin{aligned}
\epsilon_g(\theta, \tilde{\theta}) = & \frac{1}{2} \mathbb{E} \left[\left(\sum_k^K v_k g(\lambda_k) - \sum_m^M \tilde{v}_m \tilde{g}(\nu_m) \right)^2 \right] \\
= & \frac{1}{2} \sum_{k, \ell} v_k v_\ell \mathbb{E}[g(\lambda_k) g(\lambda_\ell)] + \frac{1}{2} \sum_{n, m} \tilde{v}_n \tilde{v}_m \mathbb{E}[\tilde{g}(\nu_n) \tilde{g}(\nu_m)] - \sum_{k, n} v_k \tilde{v}_n \mathbb{E}[g(\lambda_k) \tilde{g}(\nu_n)]
\end{aligned} \tag{A48}$$

Appendix B: Dynamics Results from Different Activation Function

Similar convergence results can be observed even when using the error function (erf).

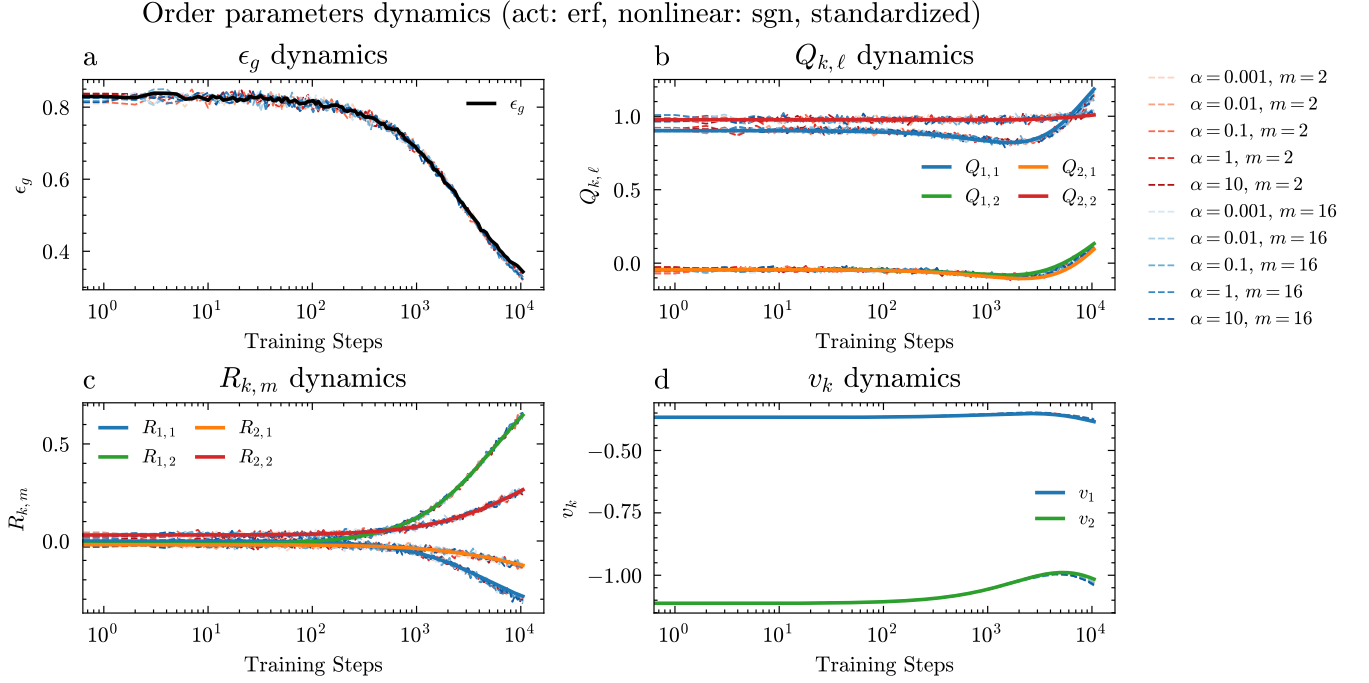


FIG. A1. Examples of dynamics under standardized Gaussian mixtures with $m = 2, m = 16$, and $\alpha = 0.001, 0.01, 0.1, 1, 10$. Dynamics of (a) generalization error ϵ_g , (b) covariance matrix Q , (c) covariance matrix R , and (d) weight of the second layer v . The SGD results are averaged over 10 runs. Using error function for teacher and student model's activation function.

Appendix C: Derivation of Gaussianity

Since the observed convergence phenomenon occurs only in the standardized setting, for consistency, we denote \mathcal{C} as its standardized version throughout this section.

1. Gaussianity of U and ν

To verify that our random variables satisfy the required conditions, we define $A_{r,i}$ in terms of \mathcal{C}_r :

$$A_{r,i} = \frac{F_{r,i}}{\sqrt{D}} \mathcal{C}_r. \quad (\text{C1})$$

Since \mathcal{C}_r is drawn from a Gaussian mixture but remains an independent random variable, the sequence $A_{r,i}$, $r = 1, 2, \dots, D$ is also independent. Applying Lindeberg's condition:

$$\lim_{D \rightarrow \infty} \frac{1}{s_{D,i}^2} \sum_{r=1}^D \mathbb{E} \left[A_{r,i}^2 \mathbf{1}\{|A_{r,i}| > \varepsilon s_{D,i}\} \right] = 0, \quad (\text{C2})$$

we rewrite the condition as follows:

$$A_{r,i}^2 \mathbf{1}\{|A_{r,i}| > \varepsilon s_{D,i}\} = \frac{F_{r,i}^2}{D} \mathcal{C}_r^2 \mathbf{1}\left\{|\mathcal{C}_r| > \varepsilon \frac{s_{D,i} \sqrt{D}}{|F_{r,i}|}\right\}. \quad (\text{C3})$$

The indicator function satisfies the inequality

$$\mathbf{1}\{|\mathcal{C}_r| > a\} \leq \frac{|\mathcal{C}_r|^2}{a^2}. \quad (\text{C4})$$

which follows from Markov's inequality. Consequently, the expectation is bounded by

$$\mathbb{E} \left[\mathcal{C}_r^2 \mathbf{1}\{|\mathcal{C}_r| > a\} \right] \leq \frac{\mathbb{E}[|\mathcal{C}_r|^4]}{a^2}, \quad \forall a > 0. \quad (\text{C5})$$

Applying Assumption V.1 and substituting $a = \varepsilon s_{D,i} \sqrt{D}/|F_{r,i}|$, we obtain

$$\mathbb{E} \left[\mathcal{C}_r^2 \mathbf{1}\left\{|\mathcal{C}_r| > \varepsilon \frac{s_{D,i} \sqrt{D}}{|F_{r,i}|}\right\} \right] \leq \frac{M_{4,C} F_{r,i}^2}{\varepsilon^2 s_{D,i}^2 D}. \quad (\text{C6})$$

As a result, the expectation term in Lindeberg's condition is bounded by

$$\mathbb{E} \left[A_{r,i}^2 \mathbf{1}\{|A_{r,i}| > \varepsilon s_{D,i}\} \right] \leq \frac{M_{4,C} F_{r,i}^4}{\varepsilon^2 s_{D,i}^2 D^2}. \quad (\text{C7})$$

Under Assumption V.2, summing over r , we obtain

$$\sum_{r=1}^D \mathbb{E} \left[A_{r,i}^2 \mathbf{1}\{|A_{r,i}| > \varepsilon s_{D,i}\} \right] \leq \frac{M_{4,C} K_{4,F}}{\varepsilon^2 s_{D,i}^2 D}. \quad (\text{C8})$$

Thus, the Lindeberg condition is bounded by:

$$\frac{M_{4,C} K_{4,F}}{\varepsilon^2 s_{D,i}^4 D} \quad (\text{C9})$$

which tends to 0 as $D \rightarrow \infty$. Hence, Lindeberg's condition is satisfied for U_i .

Similarly, the Gaussianity of ν can be derived using the same approach. By definition, ν_m is given by

$$\nu_m = \frac{1}{\sqrt{D}} \sum_{r=1}^D C_r \widetilde{W}_{m,r}. \quad (\text{C10})$$

Defining

$$B_{m,r} = \frac{\widetilde{W}_{m,r} C_r}{\sqrt{D}} \quad (\text{C11})$$

as with $A_{r,i}$, the terms $B_{m,r}$, $r = 1, 2, \dots, N$ are independent random variables since their randomness comes only from C_r . Applying Lindeberg's condition for ν_m , we get:

$$\lim_{D \rightarrow \infty} \frac{1}{\tilde{s}_{D,m}^2} \sum_{r=1}^D \mathbb{E} \left[B_{m,r}^2 \mathbf{1}\{|B_{m,r}| > \varepsilon \tilde{s}_{D,m}\} \right] = 0, \quad (\text{C12})$$

where

$$\tilde{s}_{D,m}^2 = \sum_{r=1}^D \text{Var}(B_{m,r}) = \frac{1}{D} \sum_{r=1}^D \widetilde{W}_{m,r}^2. \quad (\text{C13})$$

Using indicator function inequality, we obtain

$$B_{m,r}^2 \mathbf{1}\{|B_{m,r}| > \varepsilon \tilde{s}_{D,m}\} = \frac{\widetilde{W}_{m,r} C_r^2}{D} \mathbf{1}\left\{|C_r| > \varepsilon \frac{\tilde{s}_{D,m} \sqrt{D}}{|\widetilde{W}_{m,r}|}\right\}. \quad (\text{C14})$$

Using Assumption V.1 and Assumption V.4, we can follow the derivation for U and obtain the bound:

$$\frac{M_{4,C} \widetilde{K}_{4,\widetilde{W}}}{\varepsilon^2 \tilde{s}_{D,m}^4 D} \quad (\text{C15})$$

which tends to 0 as $D \rightarrow \infty$, confirming that ν_m is Gaussian.

2. Gaussianity of λ

Unlike U and ν , λ is not solely defined by U , as it includes $f(U)$ in its definition. Thus, its derivation requires an additional assumption, Assumption V.6. By definition, λ_k is given by

$$\lambda_k = \frac{1}{\sqrt{N}} \sum_{i=1}^N W_{k,i} \left(f(U_i) - \mathbb{E}[f(U_i)] \right). \quad (\text{C16})$$

Now, defining

$$Z_{i,k} = \frac{W_{k,i}}{\sqrt{N}} \left(f(U_i) - \mathbb{E}[f(U_i)] \right), \quad i = 1, \dots, N \quad (\text{C17})$$

where $W_{k,i}$ is deterministic value and $\mathbb{E}[f(U_i)]$ is also fixed, the randomness of $Z_{i,k}$ stems solely from $f(U_i)$.

To establish the independence of $Z_{i,k}$, it suffices to show that $f(U_i)$ is independent, which in turn requires proving the independence of U_i . Since we previously established that U_i behaves as a Gaussian in the thermodynamic limit, we can determine independence by checking for uncorrelation. The covariance of U_i is

$$\text{Cov}(U_i, U_j) = \frac{1}{D} \sum_{r=1}^D F_{r,i} F_{r,j}. \quad (\text{C18})$$

Applying Assumption II.1, we obtain $\text{Cov}(U_i, U_j) \rightarrow 0$ in thermodynamic limit for $i \neq j$, confirming the independence of $Z_{i,k}$.

Next, we check Lindeberg's condition:

$$\lim_{N \rightarrow \infty} \frac{1}{s_{N,k}^2} \sum_{i=1}^N \mathbb{E} \left[Z_{i,k}^2 \mathbf{1}\{|Z_{i,k}| > \varepsilon s_{N,k}\} \right] \rightarrow 0 \quad (\text{C19})$$

where

$$s_{N,k}^2 = \sum_{i=1}^N \text{Var}(Z_{i,k}) = \frac{1}{N} \sum_{i=1}^N W_{k,i}^2 \text{Var}(f(U_i)). \quad (\text{C20})$$

Using that indicator function is bounded as:

$$\mathbf{1}\{|Z_{i,k}| > a\} \leq \frac{|Z_{i,k}|^\delta}{a^\delta}. \quad (\text{C21})$$

for any $\delta > 0$. Setting $a = \varepsilon s_{N,k}$, we obtain

$$\mathbb{E} \left[|Z_{i,k}|^2 \mathbf{1}\{|Z_{i,k}| > \varepsilon s_{N,k}\} \right] \leq \frac{\mathbb{E} \left[|Z_{i,k}|^{2+\delta} \right]}{(\varepsilon s_{N,k})^\delta}. \quad (\text{C22})$$

Expanding the right-hand side using the definition of $Z_{i,k}$, we get

$$\mathbb{E} \left[|Z_{i,k}|^{2+\delta} \right] = \frac{|W_{k,i}|^{2+\delta}}{N^{\frac{2+\delta}{2}}} \mathbb{E} \left[|f(U_i) - \mathbb{E}[f(U_i)]|^{2+\delta} \right]. \quad (\text{C23})$$

Applying Assumption V.6

$$\mathbb{E} \left[|Z_{i,k}|^2 \mathbf{1}\{|Z_{i,k}| > \varepsilon s_{N,k}\} \right] \leq \frac{|W_{k,i}|^{2+\delta} M_{2+\delta}}{(\varepsilon s_{N,k})^\delta N^{\frac{2+\delta}{2}}}. \quad (\text{C24})$$

Summing over i and using Assumption V.5, we obtain

$$\sum_{i=1}^N \mathbb{E} \left[|Z_{i,k}|^2 \mathbf{1}\{|Z_{i,k}| > \varepsilon s_{N,k}\} \right] \leq \frac{K_{2+\delta} M_{2+\delta}}{(\varepsilon s_{N,k})^\delta N^{\frac{\delta}{2}}}. \quad (\text{C25})$$

Thus, Lindeberg's condition is bounded by:

$$\frac{1}{s_{N,k}^2} \cdot \frac{O(N^{-\delta/2})}{(\varepsilon s_{N,k})^\delta} \quad (\text{C26})$$

which tends to zero in the thermodynamic limit, confirming the Gaussianity of λ_k

3. Verification of Assumptions

In our setting, \mathcal{C}_r is independent, and the elements of the feature matrix F are sampled from a Gaussian distribution, as are the teacher weights \widetilde{W} and student weight W . Under this setup, we verify the satisfaction of our assumptions. First, Assumption V.1, the general fourth moment of a Gaussian variable is given by:

$$\mathbb{E}[X^4] = 3\sigma^4 + 6\sigma^2\mu^2 + \mu^4, \quad X \sim \mathcal{N}(\mu, \sigma^2) \quad (\text{C27})$$

Thus, \mathcal{C} drawn from a standardized Gaussian mixture with m components, we have

$$\mathbb{E}[\mathcal{C}^4] = \sum_{k=1}^m \pi_k (3\sigma_k^4 + 6\sigma_k^2\mu_k^2 + \mu_k^4) \quad (\text{C28})$$

where π_k are mixture weights and σ_k, μ_k are component parameters. The standardization condition

$$\sum_{k=1}^m \pi_k (\sigma_k^2 + \mu_k^2) \quad (\text{C29})$$

ensures that these parameters are controlled, preventing any component from having an excessively large fourth moment. Since all σ_k and μ_k are bounded in our setting, Assumption V.1 is satisfied. Next, Assumptions V.5, V.4, and V.2 case is simple. For a random variable $X \sim \mathcal{N}(0, 1)$, we have $\mathbb{E}[X^2] = 1$ and $\mathbb{E}[X^4] = 3$. By the law of large numbers, these assumptions hold with $K_{2,\cdot} = 1$ and $K_{4,\cdot} = 3$. Finally, for Assumption V.6 case, we can consider nonlinear functions such

as sigmoid, *tanh*, and sign functions, all of which are bounded, naturally satisfying Assumption V.6. Even in the case of ReLU, where input $x \sim \mathcal{N}(0, \sigma^2)$, the function corresponds to a half-Gaussian integral, which remains bounded under certain limits. Thus, Assumption V.6 holds.

Appendix D: Function Correlation in Gaussian Mixtures

Consider two random variables, u_1 and u_2 that follow Gaussian mixture distributions. Each variable is drawn from Gaussian components with probabilities π_k and π_l , respectively

$$p(u_1) = \sum_k \pi_k \mathcal{N}(\mu_k, \sigma_k^2), \quad p(u_2) = \sum_l \pi_l \mathcal{N}(\mu_l, \sigma_l^2). \quad (\text{D1})$$

For a component-wise representation, let us denote

$$u_{1,k} \sim \mathcal{N}(\mu_k, \sigma_k^2), \quad u_{2,l} \sim \mathcal{N}(\mu_l, \sigma_l^2). \quad (\text{D2})$$

Thus, the joint probability can be rewritten as

$$p(u_1, u_2) = \sum_{k,l} \pi_k \pi_l p_{kl}(u_{1,k}, u_{2,l}). \quad (\text{D3})$$

If the correlation within each component is weak, meaning $\text{Cov}(u_{1,k}, u_{2,l}) = \rho_{kl} \sigma_k \sigma_l$ with $\rho_{kl} \ll 1$, we obtain joint probability as follows:

$$p_{kl}(u_{1,k}, u_{2,l}) = \frac{1}{2\pi \sigma_k \sigma_l \sqrt{1 - \rho_{kl}^2}} \exp \left[-\frac{1}{2(1 - \rho_{kl}^2)} \left(\frac{(u_{1,k} - \mu_k)^2}{\sigma_k^2} - 2\rho_{kl} \frac{(u_{1,k} - \mu_k)(u_{2,l} - \mu_l)}{\sigma_k \sigma_l} + \frac{(u_{2,l} - \mu_l)^2}{\sigma_l^2} \right) \right] \quad (\text{D4})$$

$$= \mathcal{N}(u_{1,k}; \mu_k, \sigma_k^2) \mathcal{N}(u_{2,l}; \mu_l, \sigma_l^2) \frac{1}{\sqrt{1 - \rho_{kl}^2}} \exp(A) \exp(B). \quad (\text{D5})$$

where

$$A = \left[\frac{\rho_{kl} (u_{1,k} - \mu_k)(u_{2,l} - \mu_l)}{(1 - \rho_{kl}^2) \sigma_k \sigma_l} \right],$$

$$B = \left[-\frac{\rho_{kl}^2}{2(1 - \rho_{kl}^2)} \left(\frac{(u_{1,k} - \mu_k)^2}{\sigma_k^2} + \frac{(u_{2,l} - \mu_l)^2}{\sigma_l^2} \right) \right]. \quad (\text{D6})$$

Since ρ_{kl} is small, we neglect higher-order terms

$$\frac{1}{\sqrt{1 - \rho_{kl}^2}} = 1 + \frac{1}{2}\rho_{kl}^2 + \mathcal{O}(\rho_{kl}^4), \quad (\text{D7})$$

$$\exp \left[-\frac{\rho_{kl}^2}{2(1 - \rho_{kl}^2)} (\dots) \right] = 1 - \frac{\rho_{kl}^2}{2} + \mathcal{O}(\rho_{kl}^4), \quad (\text{D8})$$

$$\exp \left[\frac{\rho_{kl} r}{(1 - \rho_{kl}^2)} \right] = 1 + \rho_{kl} r + \mathcal{O}(\rho_{kl}^2). \quad (\text{D9})$$

where

$$r = \frac{(u_{1,k} - \mu_k)(u_{2,l} - \mu_l)}{\sigma_k \sigma_l}. \quad (\text{D10})$$

Thus, the first-order expansion of $p_{kl}(u_{1,k}, u_{2,l})$ is

$$p_{kl}(u_{1,k}, u_{2,l}) = \mathcal{N}(\mu_k, \sigma_k^2) \mathcal{N}(\mu_l, \sigma_l^2) [1 + \rho_{kl} r] + \mathcal{O}(\rho_{kl}^2). \quad (\text{D11})$$

From this, the function correlation is given by:

$$\mathbb{E}[f(u_{1,k})g(u_{2,l})] = \sum_{k,l} \pi_k \pi_l \left\{ \underbrace{\left[\int f(u_{1,k}) \mathcal{N}(u_{1,k}; \mu_k, \sigma_k^2) du_{1,k} \right] \left[\int g(u_{2,l}) \mathcal{N}(u_{2,l}; \mu_l, \sigma_l^2) du_{2,l} \right]}_{\equiv \langle f(u_{1,k}) \rangle_k \langle g(u_{2,l}) \rangle_l} \right. \quad (\text{D12})$$

$$\left. + \rho_{kl} \underbrace{\left(\int f(u_{1,k}) \frac{u_{1,k} - \mu_k}{\sigma_k} \mathcal{N}(u_{1,k}; \mu_k, \sigma_k^2) du_{1,k} \right) \left(\int g(u_{2,l}) \frac{u_{2,l} - \mu_l}{\sigma_l} \mathcal{N}(u_{2,l}; \mu_l, \sigma_l^2) du_{2,l} \right)}_{=: F_k G_l} \right\} + \mathcal{O}(\rho_{kl}^2). \quad (\text{D13})$$

where $\langle \cdot \rangle_k$ denotes the expectation with respect to the Gaussian distribution of the k -th component in the mixture. If we extend this result to vector-valued u_1 and u_2 , the computation remains unchanged, except that inner products and expectations are evaluated using matrix operations.

For instance, consider the case where u_1 follows a standard Gaussian distribution $\mathcal{N}(0, 1)$ and u_2 follows a standardized Gaussian mixture,

$$p(u_2) = \sum_l \pi_l \mathcal{N}(\mu_l, \sigma_l^2) \quad (\text{D14})$$

and $g(\cdot)$ is the identity function.

In this case, since $\mathbb{E}[u_1] = 0$ the first term vanishes, leaving the second term dominant. Additionally, F_k is simplified to $\mathbb{E}[u_1 f(u_1)]$, and the second term reduces to

$$\sum_{k,l} \pi_l \rho_l \mathbb{E}[u_1 f(u_1)] G_l, \quad (\text{D15})$$

where

$$\rho_l = \frac{\text{Cov}(u_1, u_{2,l})}{\sigma_l} \quad (\text{D16})$$

The term G_l is computed as

$$G_l = \int u_{2,l} \frac{u_{2,l} - \mu_l}{\sigma_l} \mathcal{N}(u_{2,l}; \mu_l, \sigma_l^2) du_{2,l} = \sigma_l. \quad (\text{D17})$$

Since the standardization condition ensures $\mathbb{E}[u_2] = 0$ and $\text{Var}(u_2) = 1$, we obtain

$$\sum_{k,l} \pi_l \rho_l \mathbb{E}[u_1 f(u_1)] G_l = \mathbb{E}[u_1 f(u_1)] \rho \quad (\text{D18})$$

where the total correlation coefficient ρ is

$$\rho = \frac{\text{Cov}(u_1, u_2)}{\sqrt{\text{Var}(u_1)} \sqrt{\text{Var}(u_2)}} = \text{Cov}(u_1, u_2) \quad (\text{D19})$$

Thus, the expected function activation follows:

$$\mathbb{E}[f(u_1)u_2] = \text{Cov}(u_1, u_2) \mathbb{E}[u_1 f(u_1)]. \quad (\text{D20})$$

Appendix E: Covariance Consistency under a Gaussian Mixture

As dynamic convergence is observed only in the standardized setting, we denote \mathcal{C} as its standardized version throughout this section.

By definition, Q is given by

$$Q_{k,\ell} \equiv \mathbb{E}[\bar{\lambda}_k \bar{\lambda}_\ell] = \mathbb{E}\left[\frac{1}{N} \sum_{i=1}^N \sum_{j=1}^N W_{k,i} W_{\ell,j} (f(U_i - a)(f(U_j - a)))\right]. \quad (\text{E1})$$

Here U_i is not directly sampled from a Gaussian distribution but rather from \mathcal{C}_r ,

$$U_i = \frac{1}{\sqrt{D}} \sum_{r=1}^D \mathcal{C}_r F_{r,i}. \quad (\text{E2})$$

However, as previously established, U_i follows a Gaussian distribution in the thermodynamic limit. Consequently, the result for Q remains identical to that derived in Appendix A 2, as shown by Goldt *et al.* [1]. For R , by definition, the covariance $\mathbb{E}[\bar{\lambda}_k \nu_m]$ is given by

$$\frac{1}{\sqrt{N}} \sum_{i=1}^N W_{k,i} \frac{1}{\sqrt{D}} \sum_{r=1}^D \widetilde{W}_{m,r} \mathbb{E}[f(U_i) \mathcal{C}_r]. \quad (\text{E3})$$

Given the definitions of U_i and \mathcal{C}_r , their covariance is

$$\text{Cov}(U_i, \mathcal{C}_r) = \frac{1}{\sqrt{D}} \sum_{k=1}^D F_{k,i} \mathbb{E}[\mathcal{C}_k \mathcal{C}_r]. \quad (\text{E4})$$

Since \mathcal{C}_r is independent and satisfies the standardization condition $\mathbb{E}[\mathcal{C}_r^2] = 1$, this simplifies to

$$\text{Cov}(U_i, \mathcal{C}_r) = \frac{1}{\sqrt{D}} F_{r,i}. \quad (\text{E5})$$

. Even at the component level, the mixture component weights are independent, leading to each component wise weak correlation. Thus, we can directly apply the previously derived result from Eq. (D20), setting $u_1 \rightarrow U_i$ and $u_2 \rightarrow \mathcal{C}_r$, yielding

$$\mathbb{E}[f(U_i)\mathcal{C}_r] = \frac{1}{\sqrt{D}}F_{r,i}\mathbb{E}[U_i f(U_i)]. \quad (\text{E6})$$

Substituting this into the definition of R (Eq. (E3)) confirms that R retains the same form as Eq. (11). Furthermore, since T remains unchanged during training, all covariance structures remain consistent under the standardized Gaussian mixture setting.

Appendix F: Additional Information in Pseudo-Real Dataset Experimental Setting

In this pseudo-real dataset investigation, the dimension of teacher model input C was set to $D = 500$, and the

dimension of student model input X was set to $N = 28^2$, MNIST dimension. The encoder model consisted of a hidden layer with 256 units and used the ReLU activation function. The teacher and student models followed the same architecture as in the Gaussian mixture setting, with both having hidden layer dimensions set to $K = M = 2$. Both the teacher and student models employed the same function, $\text{hardtanh}(x) = \max(-1, \min(1, x))$. The nonlinear function $f(x)$ used to generate the student input was also defined as $f(\cdot) = \text{hardtanh}(\cdot)$. During training, we used 10,000 samples of teacher model input and employed a full-batch Adam optimizer for optimization with 10^{-4} learning rate. For the SGD and ODE dynamics simulations, we used 100,000 samples, generated using the encoder model applied to the MNIST dataset. Training was conducted for 30 epochs, and at each epoch, we recorded the corresponding teacher model and teacher model input pairs. To analyze the effect of correlation strength, we repeated the training process for different values of λ_{corr} , varying it over the ranges $\lambda_{\text{corr}} = [1.1, 1.2, 1.3, 1.4, 1.5, 1.6, 1.7, 1.8, 1.9]$ and $\lambda_{\text{corr}} = [1, 2, 3, 4, 5, 6, 7, 8, 9, 10]$.

-
- [1] S. Goldt, M. Mézard, F. Krzakala, and L. Zdeborová, *Phys. Rev. X* **10**, 041044 (2020).
 - [2] T. L. H. Watkin, A. Rau, and M. Biehl, *Rev. Mod. Phys.* **65**, 499 (1993).
 - [3] H. S. Seung, H. Sompolinsky, and N. Tishby, *Phys. Rev. A* **45**, 6056 (1992).
 - [4] H. Schwarze, *J. Phys. A-Math. Gen.* **26**, 5781 (1993).
 - [5] D. Saad, *J. Phys. A-Math. Gen.* **27**, 2719 (1994).
 - [6] M. Biehl and A. Mietzner, *J. Phys. A-Math. Gen.* **27**, 1885 (1994).
 - [7] M. Biehl and P. Riegler, *Europhys. Lett.* **28**, 525 (1994).
 - [8] M. Biehl, *Europhys. Lett.* **25**, 391 (1994).
 - [9] M. Biehl and H. Schwarze, *Europhys. Lett.* **20**, 733 (1992).
 - [10] D. Saad and S. A. Solla, *Phys. Rev. E* **52**, 4225 (1995).
 - [11] D. Saad and S. Solla, in *Advances in Neural Information Processing Systems (NeurIPS)*, Vol. 8, edited by D. Touretzky, M. Mozer, and M. Hasselmo (MIT Press, 1995).
 - [12] T. M. Heskes and B. Kappen, *Phys. Rev. A* **44**, 2718 (1991).
 - [13] H. Cui, F. Krzakala, E. Vanden-Eijnden, and L. Zdeborová, in *International Conference on Learning Representations (ICLR)* (2024).
 - [14] R. Rende, F. Gerace, A. Laio, and S. Goldt, *Phys. Rev. Res.* **6**, 023057 (2024).
 - [15] R. Rende, F. Gerace, A. Laio, and S. Goldt, *Phys. Rev. Res.* **6**, 023057 (2024).
 - [16] P. L. Bartlett, P. M. Long, G. Lugosi, and A. Tsigler, *Proc. Natl. Acad. Sci. U.S.A.* **117**, 30063 (2020), <https://www.pnas.org/doi/pdf/10.1073/pnas.1907378117>.
 - [17] S. B. Korada and A. Montanari, *IEEE Trans. Inf. Theory* **57**, 2440 (2011).
 - [18] E. J. Candès and P. Sur, *Ann. Stat.* **48**, pp. 27 (2020).
 - [19] S. Goldt, M. Advani, A. M. Saxe, F. Krzakala, and L. Zdeborová, in *Advances in Neural Information Processing Systems (NeurIPS)*, Vol. 32, edited by H. Wallach, H. Larochelle, A. Beygelzimer, F. d'Alché-Buc, E. Fox, and R. Garnett (Curran Associates, Inc., 2019).
 - [20] S. Goldt, B. Loureiro, G. Reeves, F. Krzakala, M. Mézard, and L. Zdeborová, in *Proceedings of the 2nd Mathematical and Scientific Machine Learning Conference*, Proceedings of Machine Learning Research, Vol. 145, edited by J. Bruna, J. Hesthaven, and L. Zdeborová (PMLR, 2022) pp. 426–471.
 - [21] Y. Dandi, L. Stephan, F. Krzakala, B. Loureiro, and L. Zdeborová, in *Advances in Neural Information Processing Systems (NeurIPS)*, Vol. 36, edited by A. Oh, T. Naumann, A. Globerson, K. Saenko, M. Hardt, and S. Levine (Curran Associates, Inc., 2023) pp. 54754–54768.
 - [22] L. Deng, *IEEE Signal Process. Mag.* **29**, 141 (2012).
 - [23] A. Krizhevsky, *Learning Multiple Layers of Features from Tiny Images*, Technical Report (Univ. Toronto, 2009).
 - [24] P. Pope, C. Zhu, A. Abdelkader, M. Goldblum, and T. Goldstein, in *International Conference on Learning Representations (ICLR)* (2021).
 - [25] C. Fefferman, S. Mitter, and H. Narayanan, *J. Amer. Math. Soc.* **29**, 983 (2016).
 - [26] G. E. Hinton and R. R. Salakhutdinov, *Science* **313**, 504 (2006), <https://www.science.org/doi/pdf/10.1126/science.1127647>.
 - [27] G. Peyré, *Comput. Vis. Image Underst.* **113**, 249 (2009).
 - [28] A. Creswell, T. White, V. Dumoulin, K. Arulkumaran, B. Sengupta, and A. A. Bharath, *IEEE Signal Process. Mag.* **35**, 53 (2018).
 - [29] I. Goodfellow, J. Pouget-Abadie, M. Mirza, B. Xu, D. Warde-Farley, S. Ozair, A. Courville, and Y. Bengio, *Commun. ACM* **63**, 139–144 (2020).

- [30] M. Carreira-Perpinan, *IEEE Trans. Pattern Anal. Mach. Intell.* **22**, 1318 (2000).
- [31] D. W. Scott, *Multivariate density estimation: theory, practice, and visualization* (John Wiley & Sons, 2015).
- [32] I. Goodfellow, Y. Bengio, and A. Courville, *Deep Learning* (MIT Press, 2016) <http://www.deeplearningbook.org>.
- [33] M. Gabri  , *J. Phys. A-Math. Theor.* **53**, 223002 (2020).
- [34] M. Baity-Jesi, L. Sagun, M. Geiger, S. Spigler, G. B. Arous, C. Cammarota, Y. LeCun, M. Wyart, and G. Biroli, in *Proceedings of the 35th International Conference on Machine Learning (ICML)*, Proceedings of Machine Learning Research, Vol. 80, edited by J. Dy and A. Krause (PMLR, 2018) pp. 314–323.
- [35] Y. Bahri, J. Kadmon, J. Pennington, S. S. Schoenholz, J. Sohl-Dickstein, and S. Ganguli, *Annu. Rev. Condens. Matter Phys.* **11**, 501 (2020).
- [36] L. Zdeborov  , *Nat. Phys.* **16**, 602 (2020).
- [37] Q. Wang, S. R. Kulkarni, and S. Verdu, *IEEE Trans. Inf. Theory* **55**, 2392 (2009).
- [38] J. W. Lindeberg, *Mathematische Zeitschrift* **15**, 211 (1922).
- [39] H. Cram  r and H. Wold, *Journal of the London Mathematical Society* **s1-11**, 290 (1936).
- [40] M. Refinetti, S. Goldt, F. Krzakala, and L. Zdeborova, in *Proceedings of the 38th International Conference on Machine Learning (ICML)*, Proceedings of Machine Learning Research, Vol. 139, edited by M. Meila and T. Zhang (PMLR, 2021) pp. 8936–8947.
- [41] B. Loureiro, G. Sicuro, C. Gerbelot, A. Pacco, F. Krzakala, and L. Zdeborov  , in *Advances in Neural Information Processing Systems (NeurIPS)*, Vol. 34, edited by M. Ranzato, A. Beygelzimer, Y. Dauphin, P. Liang, and J. W. Vaughan (Curran Associates, Inc., 2021) pp. 10144–10157.
- [42] F. Gerace, F. Krzakala, B. Loureiro, L. Stephan, and L. Zdeborov  , *Phys. Rev. E* **109**, 034305 (2024).
- [43] V. A. Mar  chenko and L. A. Pastur, *Math. USSR Sb.* **1**, 457 (1967).